5-17-2014

Injection Timing Effects of Diesel-Ignited Methane Dual Fuel Combustion in a Single Cylinder Research Engine

Edward Scott Guerry

Injection timing effects of diesel-ignited methane dual fuel combustion in a single cylinder research engine

By

Edward Scott Guerry

A Thesis
Submitted to the Faculty of
Mississippi State University
in Partial Fulfillment of the Requirements
for the Degree of Master of Science
in Mechanical Engineering
in the Department of Mechanical Engineering

Mississippi State, Mississippi

May 2014

Injection timing effects of diesel-ignited methane dual fuel combustion in a single cylinder research engine

By

Edward Scott Guerry

Approved:

_____

Sundar R. Krishnan
(Major Professor)

_____

Kalyan K. Srinivasan
(Co-Major Professor/Graduate Coordinator)

_____

D. Keith Walters
(Committee Member)

_____

Jason M. Keith
Interim Dean
Bagley College of Engineering

Name: Edward Scott Guerry

Date of Degree: May 16, 2014

Institution: Mississippi State University

Major Field: Mechanical Engineering

Major Professor: Sundar R. Krishnan

Title of Study: Injection timing effects of diesel-ignited methane dual fuel combustion in a single cylinder research engine

Pages in Study: 79

Candidate for Degree of Master of Science

Diesel-ignited methane dual fuel combustion experiments were performed in a single cylinder research engine (SCRE). Methane was fumigated into the intake manifold and injection of diesel was used to initiate combustion. The engine was operated at a constant speed of 1500 rev/min, and diesel rail pressure was maintained at 500 bar. Diesel injection timing (SOI) was varied to quantify its impact on engine performance and engine-out $ISNO_x$, ISHC, ISCO, and smoke emissions. The SOI sweeps were performed at different net indicated mean effective pressures (IMEPs) of 4.1, 6.5, 9.5, and 12.1 bar. Intake manifold pressure was maintained at 1.5 bar for the 4.1 and 6.5 bar IMEP SOI sweeps and 1.8 bar for the 9.5 and 12.1 bar IMEP SOI sweeps. Advancing SOI to 310º and earlier resulted in reduced $ISNO_x$. However, high methane percent energy substitution (PES) resulted in high ISHC emissions especially at low IMEP.

DEDICATION

I dedicate this thesis to my wife, Josie.

ACKNOWLEDGEMENTS

I would like to acknowledge my major professor Dr. Sundar Krishnan and co-major professor Dr. Kalyan Srinivasan for the invaluable guidance, support, and inspiration they have offered me throughout my research. I would also like to acknowledge my colleagues Mostafa Shameem, Umang Dwivedi, Chad Carpenter, Dr. Andrew Polk, Kyle Hodges, Aamir Sohail, Colin Mahony, and Taylor Bohach for their support and encouragement.

This thesis is based upon research funded by the Sustainable Energy Research Center (US DOE Award # DE-FG36-06GO86025) and supported by the facilities at the Center for Advanced Vehicular Systems at Mississippi State University.

TABLE OF CONTENTS

LIST OF TABLES

LIST OF FIGURES

NOMENCLATURE

AHRR	Apparent heat release rate
ATDC	After TDC
BDC	Bottom dead center
BMEP	Brake mean effective pressure
BTDC	Before TDC
CA 10-90	Crank angle duration between locations of 10% and 90% cumulative heat release
CA5	Crank angle at which 5% of cumulative heat release occurs
CA50	Crank angle at which 50% of cumulative heat release occurs
CAD	Crank angle degree
CO	Carbon monoxide
COV IMEP	Coefficient of variation of IMEP
EGR	Exhaust gas recirculation
EOI	End of injection
FCE	Fuel conversion efficiency
FSN	Filter smoke number
HC	Unburned hydrocarbons
HCHO	Formaldehyde
ID	Ignition delay

IFCE	Indicated fuel conversion efficiency
IMEP	Indicated mean effective pressure
ISCO	Indicated specific carbon monoxide
ISHC	Indicated specific hydrocarbons
$ISNO_x$	Indicated specific oxides of nitrogen
LHV	Lower heating value
LTHR	Low temperature heat release
MPRR	Maximum pressure rise rate
NO_x	Oxides of nitrogen
PES	Percent energy substitution
PM	Particulate matter
Q_{LHV}	Mass-averaged lower heating value (kJ/kg)
SADI	Stand alone direct injection
SCRE	Single cylinder research engine
SOC	Start of combustion
SOI	Start of injection of diesel fuel
TDC	Top dead center

Subscripts:

a	Air
d	diesel
f	fuel
g	gaseous methane fuel
st	Stoichiometric

CHAPTER I

INTRODUCTION

Due to environmental and economic factors as well as increasingly strict emissions standards, internal combustion engine design and development has been the topic of much research in recent years. Compression ignition (CI) engines are known for exhibiting higher efficiency and reliability when compared to spark ignition (SI) engines. However, CI engines produce high oxides of nitrogen (NO_x) and particulate matter (PM) or soot emissions, which are a major focus in CI engine research as they are regulated emissions [Shah et al. 2006]. Expensive after-treatment systems have been designed and implemented to meet engine emissions standards. Research shows that it is challenging to simultaneously reduce NO_x and PM emissions without sacrificing efficiency.

Dual fuel engines have been the subject of much research and could be practical alternatives to the widely used diesel and gasoline engines of today. As the name implies, dual fuel engines use two fuels to produce power, and the combustion process is significantly different than that exhibited by typical diesel combustion. The primary fuel (usually methane) is fumigated a sufficient distance upstream of the intake manifold to allow for mixing with the intake air. The methane-air mixture is introduced into the cylinder during the intake stroke. Diesel fuel is directly injected into the cylinder during the compression stroke and compression-ignites which in turn ignites the surrounding methane-air mixture. Key roles in the combustion process are played by the relative

percentage of methane and diesel in the fuel mixture, diesel pilot start of injection (SOI), and availability of air [Nielsen et al. 1987, Liu and Karim 1995]. Karim described the dual fuel combustion process as occurring in three distinct stages [Karim 2003]. After the period between diesel pilot injection and ignition known as ignition delay, the diesel pilot releases energy and initiates the combustion process. Then, the surrounding methane-air mixture ignites. Finally, the combustion process continues by flame propagation through the remaining lean methane-air mixture.

There are some inherent problems affecting dual fuel engine development that need to be addressed. Although dual fuel engines prove advantageous over conventional diesel engines through higher fuel conversion efficiency at full load and lower emissions, they tend to exhibit knock at high loads and produce greater amounts of unburned hydrocarbons and carbon monoxide emissions at low loads [Korakianitis et al. 2011, Gatts et al. 2012]. Dual fuel combustion is also being studied at advanced SOIs, where homogeneous charge compression ignition (HCCI) combustion can lead to unwanted pressure waves and knock [Eng 2002]. HCCI is characterized by the mixing of fuel and air before start of combustion followed by ignition of the premixed charge as a result of temperature increase in the cylinder during the compressions stroke [Yao et al. 2009, Saxena and Bedoya 2013]. In the experiments described in this thesis, methane is mixed with air in the intake of the engine, and at very advanced SOI diesel is given sufficient time to mix with the already premixed methane-air charge. Combustion characteristics exhibit "HCCI-like" behavior at these very advanced SOI and could be considered diesel-assisted HCCI.

Natural gas, of which methane is the primary component, is an abundant and popular gaseous fuel used in dual fuel combustion research [De Carvalho Jr. 1985, Hesterberg et al. 2008, Korakianitis et al. 2011, Paul et al. 2013, Mustafi et al. 2013, Selim 2001]. High amounts of unburned methane emissions are associated with diesel-methane dual fuel combustion. Current United States Environmental Protection Agency (EPA) standards regulate the amount of non-methane hydrocarbon (NMHC) emissions, but future regulations may include limits on methane emissions.

The contributions of different engine control variables are the subject of research in diesel-ignited methane dual fuel combustion, which is the focus of this study. Liu et al. studied the effects of pilot fuel quantity in a natural gas (CNG)-diesel dual fuel engine and found that dual fuel operation resulted in higher CO emissions [Liu et al. 2013]. They also observed an average of 30 percent reduction in NO_x emissions as well as increased unburned HC emissions, 90 percent of which were unburned methane. Carlucci et al. presented experimental data from CNG-diesel dual fuel operation, which studied the effect of CNG and diesel injection pressure as well as pilot quantity at various loads and engine speeds [Carlucci et al. 2008]. They observed increased CO and HC emissions as well as decreased NO_x and PM emissions and concluded that the emissions trends were less sensitive to pilot quantity at higher engine speeds. Papagiannakis et al. analyzed diesel-ignited natural gas dual fuel operation at various proportions of natural gas substitution [Papagiannakis and Hountalas 2003, Papagiannakis and Hountalas 2004, Papagiannakis et al. 2010]. They observed an increase in CO and HC emissions as well as a decrease in NO_x and PM emissions as the percentage of natural gas substitution was increased.

Researchers are in pursuit of several strategies to resolve emissions challenges in compression ignition engines. A dual fuel combustion strategy presented in this study involves a methane-air mixture ignited using a diesel pilot. This strategy is based on the idea that in-cylinder stratification of fuel reactivity between the low-cetane primary fuel and high-cetane pilot can be used to control the partially premixed combustion process [Inagaki et al. 2006, Kokjohn et al. 2009, Splitter et al. 2011, Kokjohn et al. 2011]. Other factors that influence dual fuel combustion characteristics include partial pressure of O_2 (availability of O_2) as well as presence of diluents (affects c_p), which would alter end of compression temperatures thereby affecting start of combustion (SOC). This early injection also ensures separation of SOI from SOC, which helps to achieve lean low temperature combustion (LTC) and thereby very low NO_x and soot emissions. The advanced low pilot ignited natural gas (ALPING) combustion concept was proposed [Srinivasan et al. 2004, Krishnan et al. 2004, Srinivasan et al. 2006, Qi et al. 2007, Srinivasan et al. 2007] to achieve better efficiency and very low NO_x emissions. However, it resulted in high amounts of unburned hydrocarbon emissions [Krishnan et al. 2004]. Hot exhaust gas recirculation (EGR) and intake charge heating were later used to achieve reduced hydrocarbon emissions along with low NO_x and high efficiency benefits of ALPING combustion [Qi et al. 2007].

Another type of exhaust emission included in this study is engine-out PM number concentration and size distribution. Although PM number concentrations are not currently regulated by the EPA, future standards are likely to include restrictions. Limited research [Prikhodko et al. 2011, Prikhodko et al. 2010, Kolodziej et al. 2013] has investigated particle number concentrations and particle size distribution in a dual fuel

engine in which a high-cetane pilot fuel is used to ignite a mixture of low-cetane fuel and air. Those studies focused on diesel-ignited gasoline dual fueling (also termed reactivity controlled compression ignition or RCCI). However, a recent study [Zhou et al. 2013] examined PM number concentrations in a micro-pilot-ignited natural gas engine. They concluded that the number of particles was more sensitive to pilot injection timings, especially SOI advanced beyond 20º before top dead center (BTDC). This conclusion is of particular interest to this study, which will explore SOI as early as 260º.

Sayin and Canaksi studied diesel-ignited methane dual fuel combustion in a naturally aspirated single cylinder CI engine and limited SOI to between 339º and 327º [Sayin and Canaksi 2009]. Polk et al. [Polk et al. 2013] and Gibson et al. [Gibson et al. 2011] studied diesel-ignited methane dual fuel combustion in a 1.9L Volkswagen turbocharged direct-injected engine, which utilized the stock engine control unit (ECU). The performance during those experiments benefited from a boosted intake pressure as well as EGR. However, the ability to control diesel SOI and diesel injection pressure was at the mercy of the stock ECU, which limited the PES.

The experiments presented in this study were performed on a single cylinder research engine (SCRE) without EGR. Dwivedi performed experiments on the same SCRE at a single load of 5.2 bar IMEP while varying SOI [Dwivedi 2013]. The objectives of this study are as follows:

1. To leverage engine control parameters such as diesel SOI, diesel injection pressure, intake manifold pressure, and percentage energy substitution of methane to achieve a timing sweep at both advanced SOI (as early as

260º) as well as SOI closer to TDC (as late as 360º) for a range of engine loads.

2. To investigate the effects of diesel pilot SOI on performance and emissions characteristics of diesel-methane dual fuel combustion over a range of engine net indicated mean effective pressure (IMEP) conditions (4.1 bar to 12.1 bar IMEP) in the SCRE at a constant speed of 1500 rev/min without EGR.

CHAPTER II

EXPERIMENTAL SETUP

Figure 2.1 shows a schematic of the experimental setup, and the engine specifications can be found in Table 2.1.

Table 2.1 Engine Specifications

Parameter	**Value**
Engine Type	RSi-130 DV11 Single cylinder research engine, compression-ignition
Bore × Stroke	128 mm × 142 mm
Connecting rod length	228 mm
Displaced Volume	1827 cm^3
Compression ratio (nominal)	17.1 : 1
Valve train system	4-valve, OHV
Intake valve open	32º
Intake valve close	198º
Exhaust valve open	531º
Exhaust valve close	14º
Diesel fuel injection system	CP3 Bosch common-rail
Methane fuel system	Fumigation into intake manifold
Maximum speed	1900 rev/min

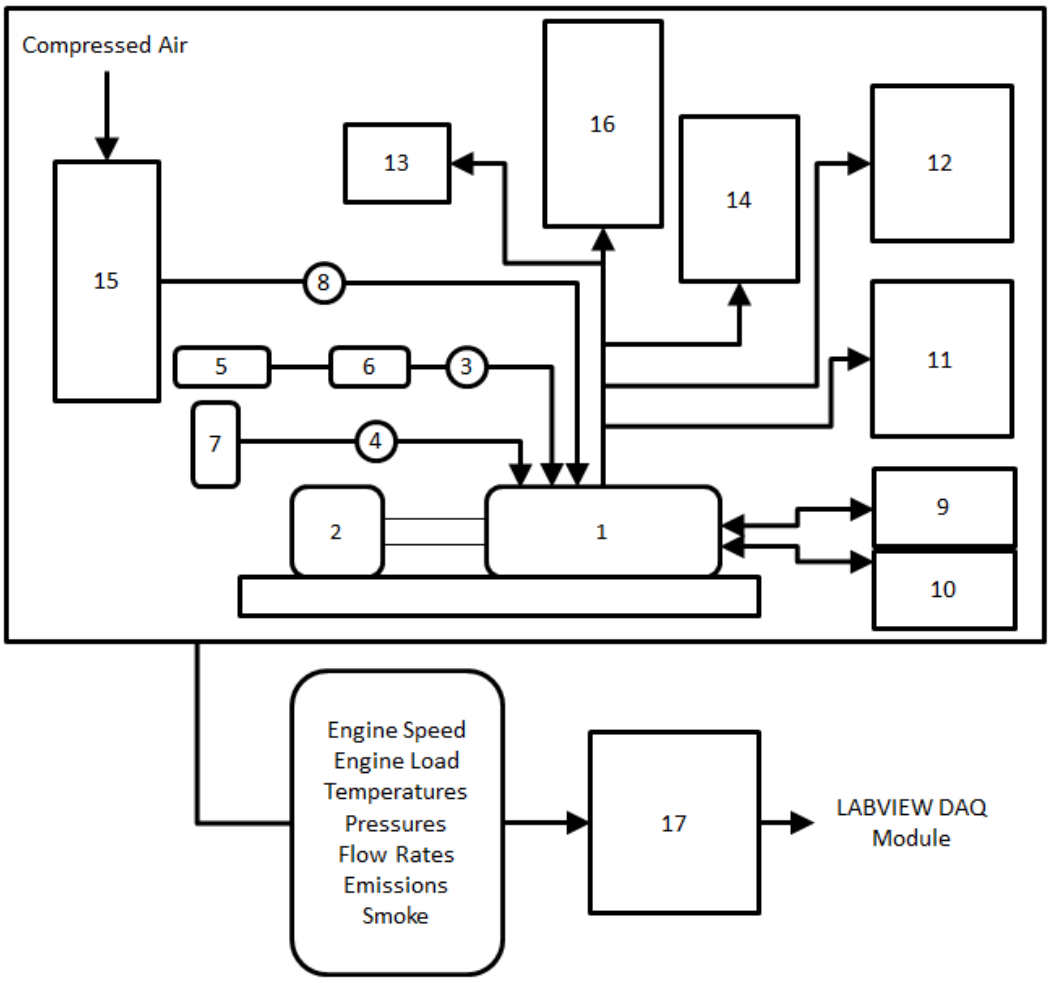

Figure 2.1 Experimental setup of the single cylinder research engine

The engine was coupled to a 250 hp AC regenerative engine dynamometer and a Dyne Systems Inter-Loc V controller, which provided torque and speed measurements and control. A Bosch CP3 common-rail pump and a solenoid-actuated injector were used

to achieve direct injection of diesel fuel. A Drivven (National Instruments) stand-alone diesel injection (SADI) driver coupled with CALVIEW software was used to control crank angle-resolved diesel injections. An electronic HANBAY needle valve (Hanbay, Inc., Model MCM-050AB) was used to control the methane flow rate into the engine intake.

2.1 Data Acquisition

Intake, exhaust, coolant, and oil temperatures were measured using Type-K thermocouples. Coolant and oil inlet temperatures of about 80ºC were maintained throughout the experiments. Gaseous and exhaust emissions were measured downstream of the exhaust manifold using an emissions sampling trolley and a six-gas emissions bench (EGAS 2M) manufactured by Altech Environment S.A. An AVL SESAM i60 FT Fourier Transform Infrared (FTIR) analyzer was used for additional speciation of the gaseous exhaust emissions. Smoke was measured in filter smoke number (FSN) units using an AVL 415S variable sampling smoke meter. A rotating disk thermo-dilutor (TSI model 3090) with a dilution factor of 1:1870 coupled with an engine exhaust particle sizer (EEPS) spectrometer was used to measure particle number concentrations and size distributions in the exhaust stream. The dilution factor was determined based on preliminary experiments wherein a ten-hole disk was used to analyze high smoke and low smoke conditions while staying within the upper and lower boundaries of the analyzer.

The in-cylinder pressure was measured using a Kistler model 6052C pressure sensor and a Kistler 5010B type charge amplifier. Needle lift was measured using a Wolff hall effect sensor. The in-cylinder pressure and needle lift sensors were phased with respect to crank angle using a BEI incremental shaft encoder with 0.1 crank angle

degree (CAD) resolution (3600 pulses per revolution) coupled to the engine crankshaft. Using absolute crank angle convention, 0º is interpreted as gas exchange TDC, and 360º is interpreted as compression TDC. An external air compressor and a heatless desiccant air dryer were employed to simulate intake charge boost. Intake air mass flow rate was measured using a calibrated FlowMaxx sonic orifice coupled with measurements of upstream pressure and temperature. To ensure a "choked" or "sonic" state at all times, an upstream to downstream pressure ratio of 1.2 or greater was maintained across the orifice. Intake air temperature was maintained between 27ºC and 32ºC and was fairly constant for a given IMEP. Micro Motion coriolis mass flow meters with 0.56 percent and 0.35 percent accuracies (of reading), respectively were used to measure both the methane (primary) and diesel (secondary) mass flow rates. Relevant instrumentation details are given in Table 2.2.

Table 2.2 Instrumentation Specifications

Data Type	Sensor/Instrument	Type	Accuracy
Temperature	Thermocouple	K	Greater: 1.1ºC or 0.4%
Pressure for venturi	Omega MM Series	Differential	0.08% FS BSL
Mass air flow	Flowmaxx	Venturi	
Mass diesel flow	Micro Motion	Coriolis	0.35% of reading
Mass methane flow	Micro Motion	Coriolis	0.56% of reading
Smoke	AVL415S	Filter	0.005 FSN + 3% of reading
NO_x	ESA EGAS 2M	CLD	1% FS
NO	ESA EGAS 2M	CLD	1% FS
THC	ESA EGAS 2M	FID	1% FS
CO-low	ESA EGAS 2M	NDIR	1% FS
CO-high	ESA EGAS 2M	NDIR	1% FS
CO_2	ESA EGAS 2M	NDIR	1% FS
Cylinder Pressure	Kistler 6052C	Piezoelectric	Linearity: 0.3% FSO
Needle Lift	Wolff Controls	Hall Effect	

2.2 Experimental Procedure

As mentioned earlier, the objective of this study is to investigate the effects of SOI on the performance and emissions characteristics of diesel-methane dual fuel combustion in the SCRE without EGR. To achieve this objective the engine was operated at four constant loads (4.1, 6.5, 9.5, and 12.1 bar IMEPs) and a constant speed of 1500 rev/min while varying SOI. Preliminary experiments were performed to determine "optimal" operating parameters (e.g., diesel injection pressure, intake boost pressure, etc.) for each SOI sweep. Based on these preliminary experiments and considering the wide range of SOIs investigated in this study, the diesel injection pressure was set to 500 bar for all of the experiments to avoid excessively high cylinder pressures

and pressure rise rates and to yield reasonably low indicated specific oxides of nitrogen ($ISNO_x$) and PM emissions.

The parameters of each experiment are summarized in the experimental matrix in Table 2.3. For the 4.1 and 6.5 bar IMEP SOI sweeps, the intake pressure was maintained at 1.5 bar and methane PES was set to 80 percent. The intake pressure was chosen to avoid misfire at advanced SOIs. The PES was limited by excessive indicated specific hydrocarbons (ISHC) and indicated specific carbon monoxide (ISCO) emissions as well as high coefficient of variation of IMEP (COV IMEP) at advanced SOIs. The timing sweeps were performed at 260º-360º SOI.

For the 9.5 bar IMEP SOI sweep, the intake pressure was increased to 1.8 bar and PES was increased to 88 percent. Increased intake pressure was required to avoid high COV IMEP at advanced SOIs. An increase in PES was required in order to avoid high in-cylinder pressures at advanced SOIs. The timing sweep was performed at 330º-350º and 260º-310º SOI. The SOI of 360º was omitted due to excessive ISHC emissions while 320º SOI was omitted due to excessive in-cylinder pressure and maximum pressure rise rate (MPRR).

For the 12.1 bar IMEP SOI sweep, intake pressure was maintained at 1.8 bar and PES was increased to 95 percent. PES was increased to avoid high in-cylinder pressures and MPRRs at advanced SOIs. Furthermore, PES was limited by diesel pilot injection pressure control. These experiments were performed with a standard common-rail diesel injection system. Therefore, it was difficult to maintain constant injection pressures for very small pilot quantities. These experiments were performed at 340º-350º and 260º-

310º SOIs. The SOI of 360º was omitted due to excessive ISHC emissions. The SOIs of 320º and 330º were omitted due to excessive in-cylinder pressure and MPRR.

Table 2.3 Experimental Matrix

Engine Load (IMEP)	SOI	Constant Parameters
4.1 bar	260º - 360º	P_{in} = 1.5 bar PES = 80%
6.5 bar	260º - 360º	P_{in} = 1.5 bar PES = 80%
9.5 bar	260º - 310º 330º - 350º	P_{in} = 1.8 bar PES = 88%
12.1 bar	260º - 310º 340º - 350º	P_{in} = 1.8 bar PES = 95%
For all experiments: Engine speed = 1500 rev/min, Rail pressure = 500 bar		

For ease of analysis, relevant combustion parameters such as equivalence ratio (Φ), percent energy substitution (PES), ignition delay (ID), and combustion efficiency are defined below:

$$\Phi = \frac{\left(A_F\right)_{st-tot}}{\left(\frac{\dot{m}_a}{\dot{m}_d + \dot{m}_g}\right)} \qquad PES = \frac{\dot{m}_g LHV_g}{\dot{m}_d LHV_d + \dot{m}_g LHV_g} \times 100\% \tag{2.1}$$

$$\tag{2.2}$$

$$ID = CA5 - SOI \tag{2.3}$$

$$\eta_c = 1 - \frac{\sum_i x_i Q_{LHV_i}}{[\dot{m}_f/(\dot{m}_a + \dot{m}_f)]\, \dot{Q}_{LHV_f}} \tag{2.4}$$

$$AHRR(\theta) = \frac{\gamma}{\gamma - 1} P \frac{dV}{d\theta} + \frac{1}{\gamma - 1} V \frac{dP}{d\theta} \tag{2.5}$$

$$\gamma(T) = 1.338 - 6 \times 10^{-5} T + 1 \times 10^{-8} T^2 \tag{2.6}$$

In Equations 2.1 and 2.2, $\dot{m}$ refers to the mass flow rates of diesel (subscript *d*), gaseous methane fuel (subscript *g*), and air (subscript *a*), and *LHV* refers to the corresponding fuel lower heating values. Stoichiometric air-fuel ratio $(A/F)_{st\text{-}tot}$ is defined as the stoichiometric air required for complete oxidation of both the pilot and the main fuels into CO_2 and H_2O. Therefore, $(A/F)_{st\text{-}tot}$ is dependent on the PES of methane. The start of combustion (SOC) is defined as CA5, or the crank angle at which 5 percent of cumulative heat release occurs. Combustion duration (CA 10-90) can be defined as the crank angle duration between the locations of 10 percent and 90 percent cumulative heat release rate.

In equation 2.4 [Heywood 1998], which represents combustion efficiency (η_c), x_i are the mass fractions of HC, CO, and H_2, Q_{LHVi} are the lower heating values of these species, and "f" and "a" denote fuel and air, respectively. Combustion efficiency is usually calculated based on the exhaust concentrations of CO, HC, H_2 and PM emissions and their respective lower heating values [Heywood 1998]. In this study only the measured CO and HC concentrations and the H_2 mass fractions estimated from stoichiometry are used in the combustion efficiency calculations. Following Heywood [Heywood 1998], the lower heating values for CO and H_2 are assumed to be 10.1 MJ/kg and 120 MJ/kg, respectively. The concentration of HC in the exhaust is not known from the six-gas emissions bench measurements, but since the lower heating value of HC is quite similar to that of the fuel, Heywood recommends using the lower heating value of the fuel for HC in the combustion efficiency calculations. However, since two fuels are used in dual fueling, the exhaust HC can theoretically originate from both fuels; therefore, the combined mass-fraction-weighted lower heating value of "the fuel mixture" (i.e., mass-fraction-weighted average of 42.6 MJ/kg for diesel and 50 MJ/kg for methane) is used for the exhaust HC. The relative mass fractions of diesel and methane change with PES, and consequently, the estimated lower heating value of the exhaust HC ranges from 48.5 MJ/kg (for 80 PES) to 49.6 MJ/kg (for 95 PES).

Apparent heat release rate (AHRR) was calculated using Equation 2.5 [Heywood 1998]. Gamma (γ), the ratio of specific heats, was determined using equation 2.6 based on global in-cylinder temperature (T) [Brunt 1998]. The instantaneous cylinder pressure (P) was measured at 0.1 CAD resolution. The rate of change of volume with respect to crank angle ($dV/d\theta$) was calculated using cylinder geometry and piston position. The

instantaneous volume (V) was determined using known engine geometry values such as compression ratio, bore, stroke, and connecting rod length coupled with engine crankshaft position measurements. The rate of change of pressure with respect to crank angle ($dP/d\theta$) was calculated using crank angle-resolved cylinder pressure data.

CHAPTER III

DIESEL-METHANE DUAL FUELING

3.1 4.1 bar IMEP: Performance and Emissions

The engine was operated at 4.1 bar IMEP, 1500 rev/min and 80 PES while diesel pilot SOI was varied from 260º to 360º. The diesel injection pressure and intake boost pressure were maintained at 500 bar and 1.5 bar, respectively, and no EGR was used.

3.1.1 Apparent Heat Release Rate and Cylinder Pressure

Figures 3.1 and 3.2 show the cylinder pressure and AHRR histories for various SOIs. Peak AHRR first advances for SOIs between 360º to 330º and then retards as SOI is advanced from 320º to 260º. As SOI is advanced from 330º to 320º, the shape of the AHRR curve and combustion characteristics change significantly. For this reason and for easier reading of results, cylinder pressure profiles and AHRR are plotted in two different groups.

For SOI between 360º and 330º, the AHRR curves exhibit two distinct stages of heat release and no significant low temperature heat release (LTHR) peak. The absence of LTHR at retarded SOIs can be explained as follows. For these more retarded SOIs there is little or no separation between end of injection (EOI) and SOC. Figure 3.3 shows the crank angle duration between EOI and SOC (EOI-SOC) and ignition delay for each SOI. Furthermore, at these retarded SOIs diesel is injected at relatively higher in-

cylinder temperatures of around 800 K as shown in Figure 3.12 (a). Previous studies found that LTHR is more likely to occur at temperatures below 850 K [Saxena and Bedoya 2013]. The relatively higher temperatures at retarded SOIs could possibly suppress LTHR and lead directly to hot ignition.

As SOI is advanced earlier in the compression stroke, the separation between EOI and SOC becomes greater. At 320º SOI, fuel injection ends at 330º and the main combustion event starts at 347º which corresponds to approximately 17 CAD difference between SOC and EOI. As the SOI is advanced to 300º, LTHR is still present as the separation increases from 17 CAD to approximately 52 CAD.

As SOI is advanced further from 300º to 260º, the magnitude of heat release increases and the peak heat release is phased after TDC. Furthermore, as SOI is advanced from 300º to 260º, the magnitude of LTHR decreases and a "well-mixed" combustion of diesel-methane is observed. The decreasing magnitude of LTHR could possibly be the result of the diesel being "too well-mixed" with the methane-air charge. Although the in-cylinder temperatures are relatively lower and would not suppress LTHR, the increased time available for mixing could inhibit heat release until hot ignition.

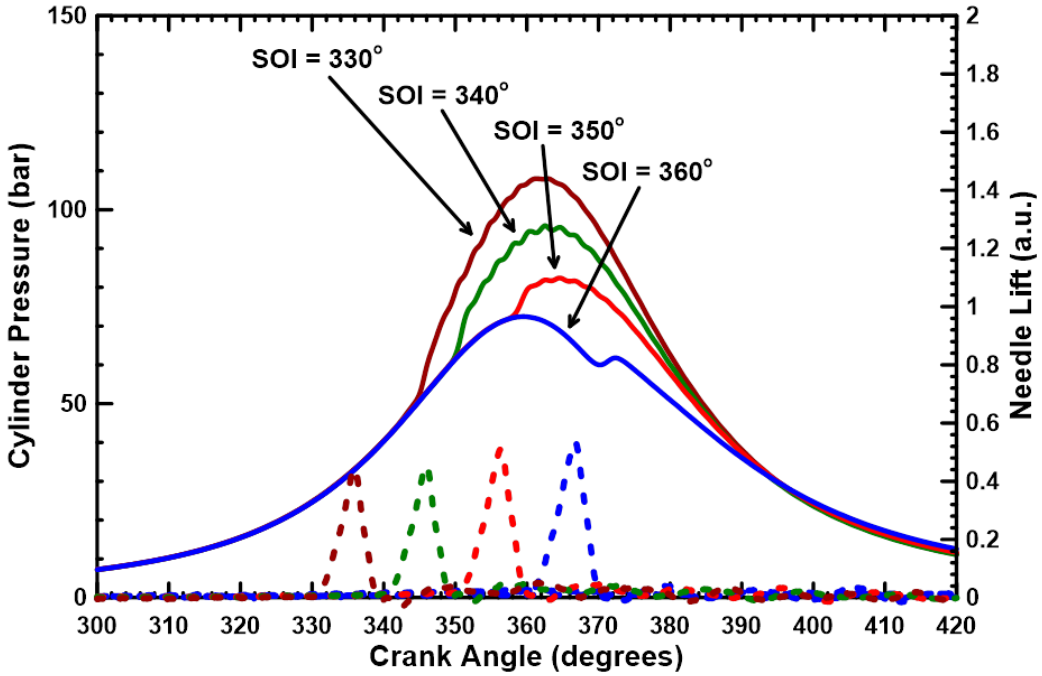

(a)

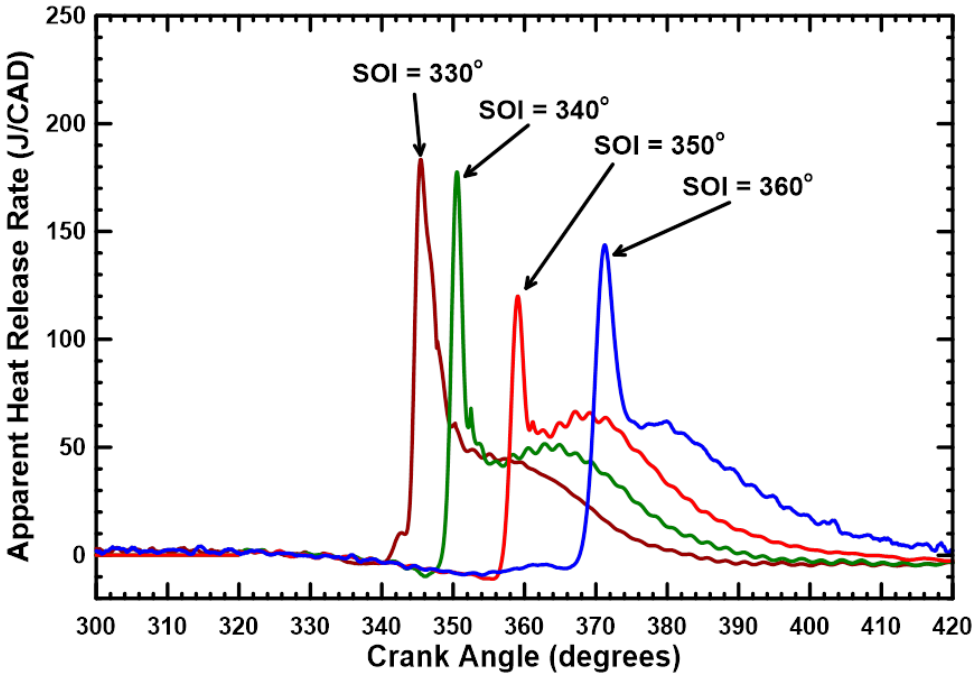

(b)

Figure 3.1 (a) Cylinder pressure histories and (b) crank angle-resolved heat release rates at late SOI at 4.1 bar IMEP, 80 PES, N=1500 rev/min, P_{in}=1.5 bar

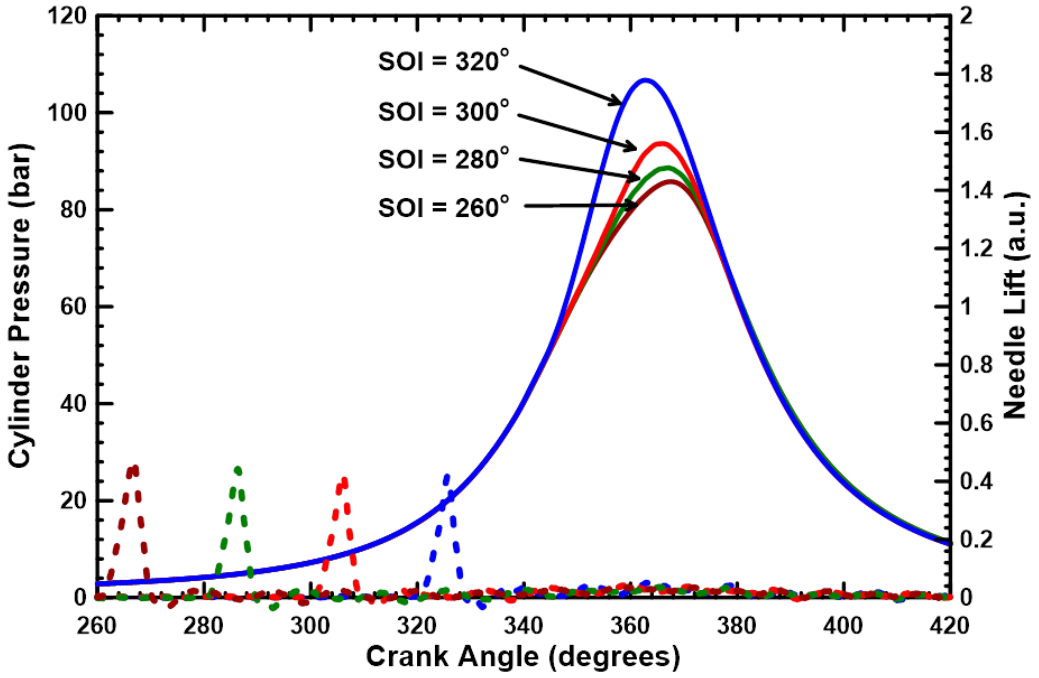

(a)

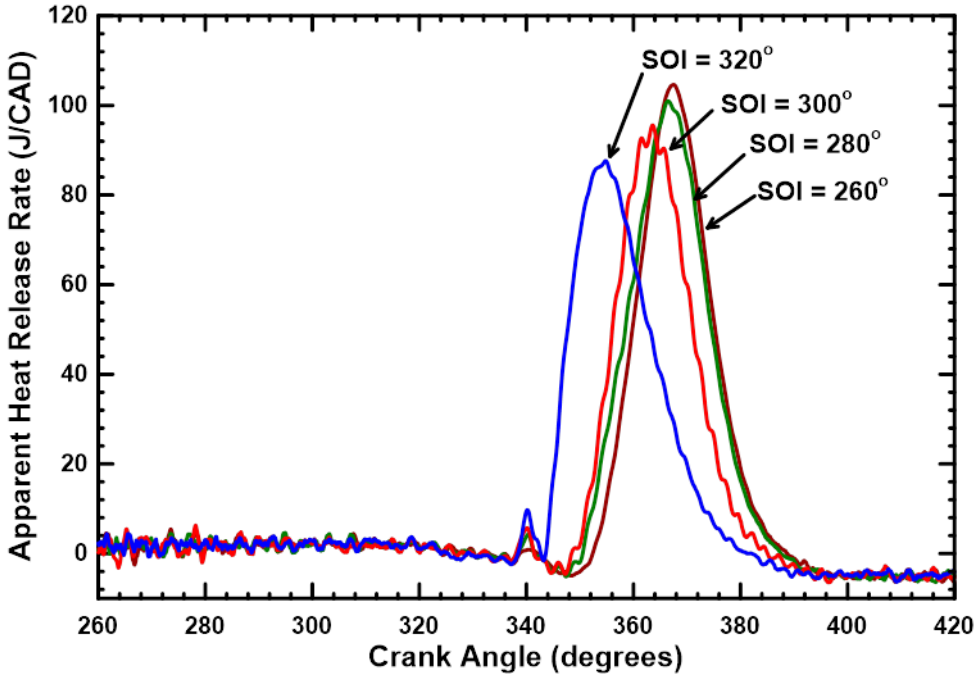

(b)

Figure 3.2 (a) Cylinder pressure histories and (b) crank angle-resolved heat release rates at early SOI at 4.1 bar IMEP, 80 PES, N=1500 rev/min, P_{in}=1.5 bar

3.1.2 Ignition Delay, Maximum Pressure Rise Rate, and Rate of Combustion

Figure 3.3 shows the EOI-SOC and ignition delay, and Figure 3.4 shows the COV IMEP and MPRR for each SOI. As SOI is advanced beyond 310º, a sharp increase in COV IMEP is observed, possibly due to the onset of misfire. For SOI in the range of 320º to 350º the highest MPRRs are observed, which correlates with the phasing of combustion close to or before TDC as shown in Figure 3.5. As SOI is advanced beyond 330º, a steady increase in ignition delay is observed. This trend may be attributed to decreasing in-cylinder bulk gas temperatures at SOI which would allow for increasingly premixed conditions.

Figure 3.5 shows the start of combustion (CA5), combustion phasing (CA50), and the combustion duration (CA10-90) for each SOI. A decrease of CA10-90 is observed from about 27 degrees to about 15 degrees when SOI is advanced from 360º to 310º and then remains between 15 and 17 degrees for SOI between 300º and 260º. A relatively consistent CA10-90 at advanced SOIs might be attributed to “well-mixed”, “HCCI-like” combustion. CA50 shifts from after TDC to before TDC when SOI is advanced from 360º to 330º and then shifts back after TDC as SOI is advanced further. This combustion phasing trend likely leads to the high MPRRs shown in Figure 3.4 at those conditions. At SOI more advanced than 320º, combustion becomes more “homogeneous” and starts closer to TDC leading to relatively lower MPRR.

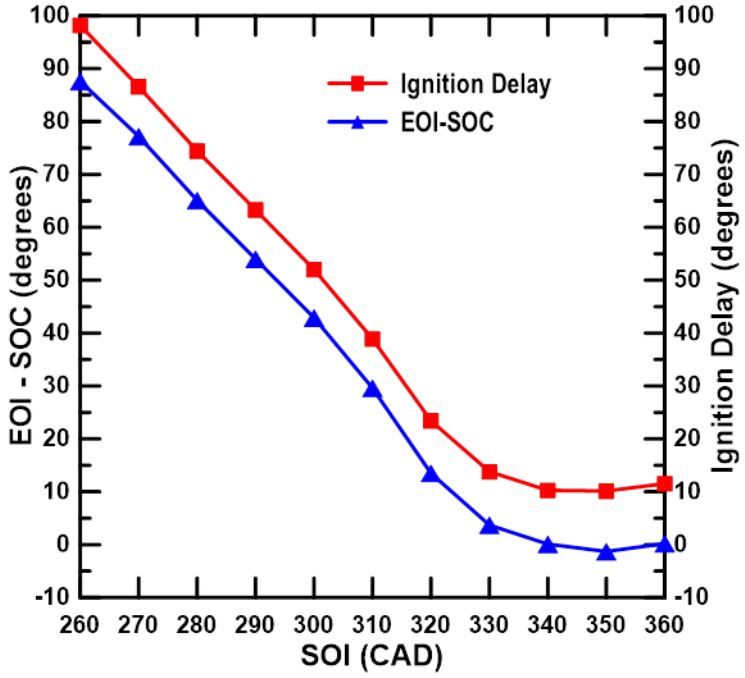

Figure 3.3 EOI-SOC and Ignition Delay at various SOIs at 4.1 bar IMEP, 80 PES, N=1500 rev/min, P_{in}=1.5 bar

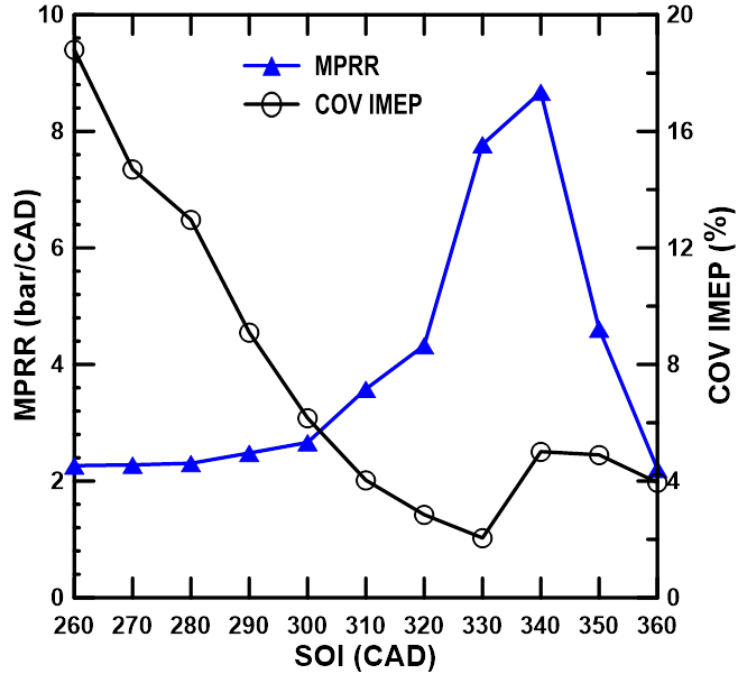

Figure 3.4 COV IMEP and MPRR at various SOIs at 4.1 bar IMEP, 80 PES, N=1500 rev/min, P_{in}=1.5 bar

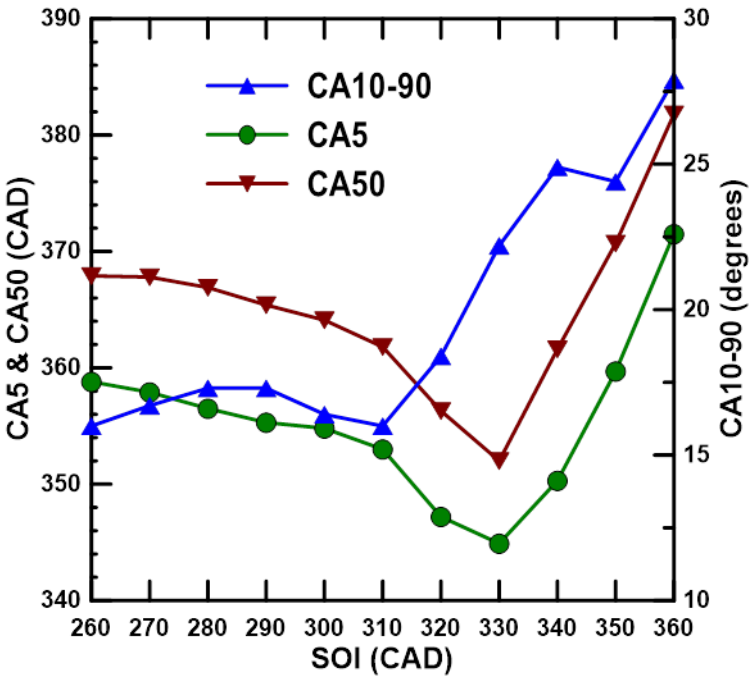

Figure 3.5 CA5, CA50 and CA10-90 at various SOIs at 4.1 bar IMEP, 80 PES, N=1500 rev/min, P_{in}=1.5 bar

3.1.3 Fuel Conversion Efficiency and Combustion Efficiency

Figure 3.6 shows the indicated fuel conversion efficiency (IFCE) and combustion efficiency between 360º and 260º SOI. Combustion efficiency decreases as SOI is advanced from 360º to 340º, then increases and reaches a peak value of about 75.5 percent at 300º SOI. An increase in combustion efficiency at advanced SOI could possibly be attributed to increasingly "well-mixed" conditions. However, at very advanced SOIs, a decrease in combustion efficiency is observed, which may indicate "too well-mixed" conditions. An increase in IFCE is observed from about 21 percent at 360º SOI to about 36 percent at 300º SOI followed by a decrease in IFCE as SOI is advanced further. This increase in IFCE may be attributed to the phasing of CA50 closer to TDC.

As SOI is advanced from 300º to 260º IFCE decreases, which could be attributed to the combined effect of CA50 moving away from TDC and decreasing combustion efficiency.

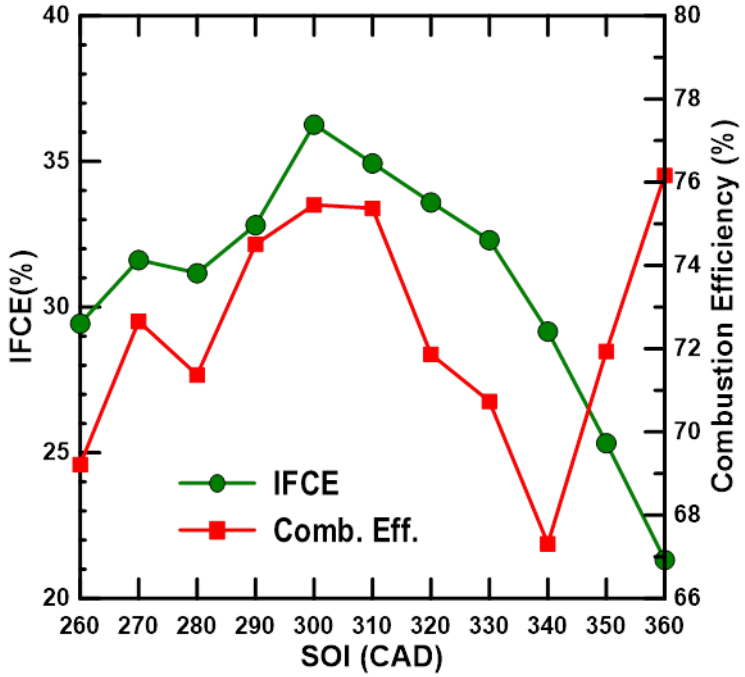

Figure 3.6 Combustion and net indicated fuel conversion efficiencies at various SOIs at 4.1 bar IMEP, 80 PES, N=1500 rev/min, P_{in}=1.5 bar

3.1.4 Emissions

Figure 3.8 shows indicated specific oxides of nitrogen ($ISNO_x$) and smoke trends for various SOIs. As SOI is advanced from 360º to 340º, the $ISNO_x$ emissions steeply increase from about 3.5 g/kWh to about 11.5 g/kWh. However, when SOI is advanced further, the $ISNO_x$ values significantly decrease to around 0.15 g/kWh and remain low until 260º SOI. Smoke emissions are less than 0.05 FSN for the duration of the SOI sweep. This may be attributed to predominately lean premixed combustion conditions fostered by the high percentage of methane energy substitution of 80 PES. Equivalence

ratios for methane-air and diesel-methane-air mixtures at each SOI are shown in Figure 3.7. The very low $ISNO_x$ level at sufficiently early SOIs is a consequence of increased residence time for mixing of diesel fuel with the lean methane-air charge. As more time for mixing is allowed before combustion begins, the in-cylinder fuel-air mixture becomes increasingly homogeneous, which may lead to lower local temperatures. In this regard, it is important to note that the simultaneous reduction of $ISNO_x$ and smoke is indicative of LTC. As mentioned earlier, the combination of adequate time available for pre-mixing and relatively lower in-cylinder temperatures play a role in promoting LTHR.

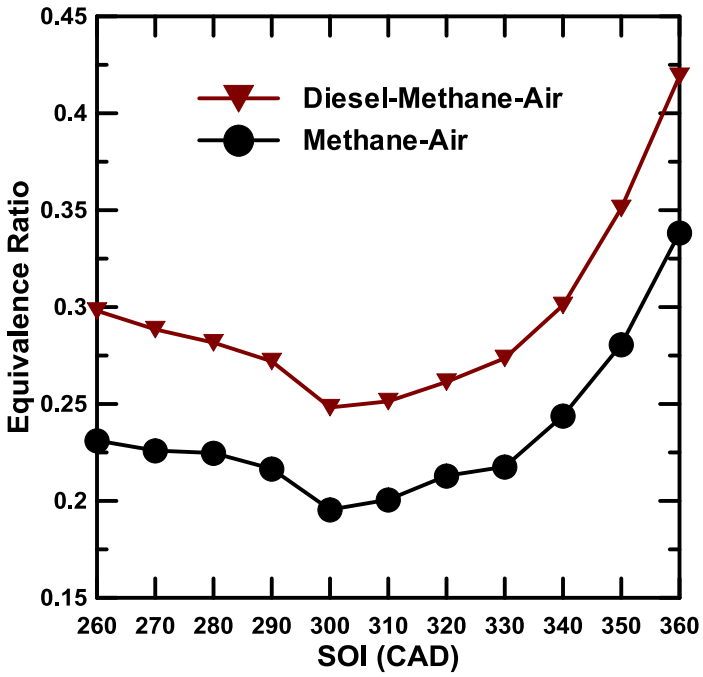

Figure 3.7 Equivalence ratio for methane-air and diesel-methane-air mixtures at various SOIs at 4.1 bar IMEP, 80 PES, N=1500 rev/min, P_{in}=1.5 bar

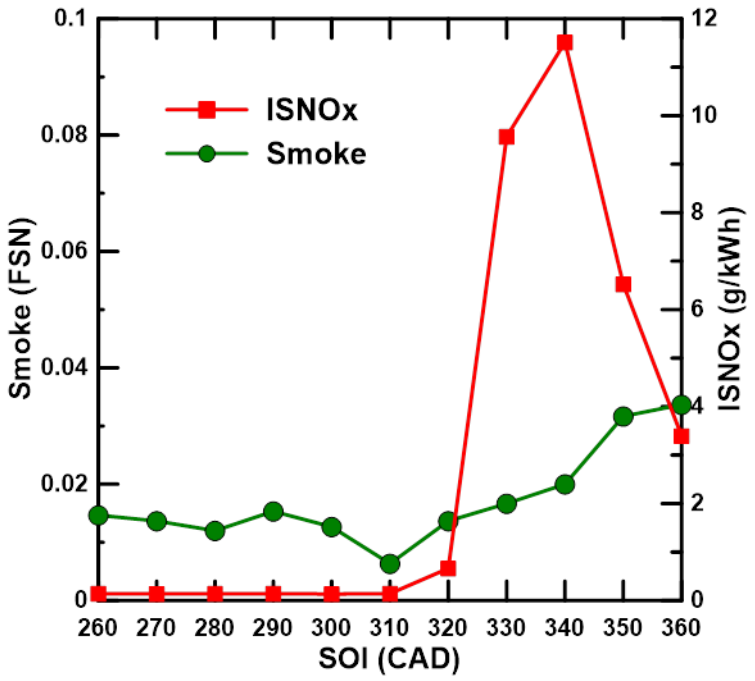

Figure 3.8 $ISNO_x$ and smoke emissions at various SOIs at 4.1 bar IMEP, 80 PES, N=1500 rev/min, P_{in}=1.5 bar

Figure 3.9 shows the ISHC and ISCO, and Figure 3.10 shows the $ISCO_2$ and formaldehyde (HCHO) emissions trends between 360º and 260º SOI. A decrease in ISCO emissions is observed from about 30 g/kWh at 360º to 15 g/kWh at 320º followed by an increase to 70 g/kWh at 260º. A decrease in ISHC emissions is observed from 120 g/kWh at 360º to about 45 g/kWh at 300º followed by an increase to nearly 80 g/kWh at 260º. The percentage of methane present in the total ISHC emissions was extremely high for all SOI. However, the actual percentage cannot be quantified from the data collected because it is beyond the scale range of the AVL FTIR analyzer.

Another species of interest measured by the AVL FTIR is HCHO. Figure 3.10 shows a steep increase in HCHO emissions from about 100 parts per million (ppm) to about 350 ppm when SOI is advanced from 320º to 260º. HCHO is formed due to

partially oxidized hydrocarbon fuel (methane) [Alzueta and Glarborg 2003]. Unburned or partially oxidized hydrocarbons are a consequence of dual fuel LTC at low loads, which causes concern, as HCHO emissions are an environmental concern (contributing to photochemical smog) and may have carcinogenic effects.

Temperature has a significant influence on the rate of HC and CO oxidation. At retarded SOIs between 360º and 340º as well as more advanced SOIs between 290º and 260º, peak in-cylinder bulk temperatures are relatively lower, which would inhibit the oxidation of HC and CO. Furthermore, major sources of unburned hydrocarbons are crevices. At more retarded SOI CA50 is phased well after TDC, so crevice hydrocarbons are not oxidized manifesting in increased ISHC emissions. At very advanced SOIs between 300º and 260º, an increasing trend in ISHC and ISCO is observed. As SOI is advanced, diesel is injected into progressively less dense methane-air mixtures. This could allow longer diesel spray penetration, which would increase the likelihood of wall or piston impingement. Therefore, a significant amount of diesel fuel can escape into relatively cooler boundary layers in the cylinder and not participate in the ignition of the premixed methane-air mixture. The lack of availability of more reactive diesel fuel increasingly impedes the combustion of the lean premixed methane-air mixture, which results in increased unburned and/or partially oxidized fuel manifesting as increased ISHC and ISCO emissions.

For SOIs between 330º and 320º ISCO emissions are fairly low. This may be attributed to the CA50 being phased closer to TDC, which could contribute to higher in-cylinder bulk temperatures to promote CO oxidation. To support this theory, bulk gas temperatures for different SOIs are plotted in Figure 3.12. For more retarded SOIs,

overall bulk gas temperatures during the combustion process are lower than those for SOIs between 320º and 260º. For SOIs ranging from 320º to 260º, peak bulk temperatures are around 1200 K. As SOI is advanced beyond 320º, ISCO emissions exhibit a steeper increase than ISHC emissions, which could be attributed to a competition between HC and CO oxidation. It is evident that the primary product of fuel oxidation is CO. Therefore, the combustion process produces a significant amount of CO. However, the oxidation of CO into CO_2 occurs later in the overall reaction process. Because HC oxidation is much faster than CO oxidation [Glassman 1996], CO oxidation does not start until all of the fuel and intermediate hydrocarbons are consumed. CO to CO_2 conversion is inhibited at lower in-cylinder bulk temperatures consequently freezing CO chemistry manifesting as higher ISCO emissions.

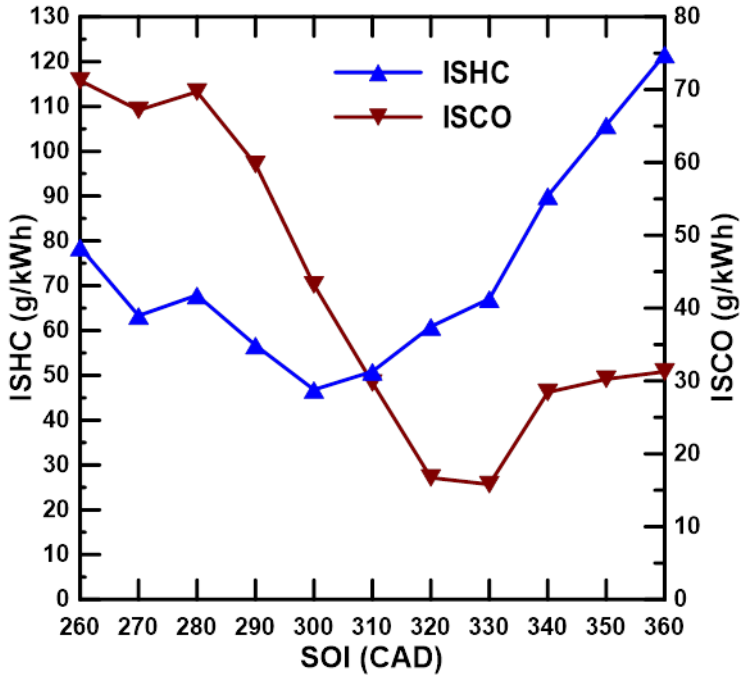

Figure 3.9 ISHC and ISCO emissions at various SOIs at 4.1 bar IMEP, 80 PES, N=1500 rev/min, P_{in}=1.5 bar

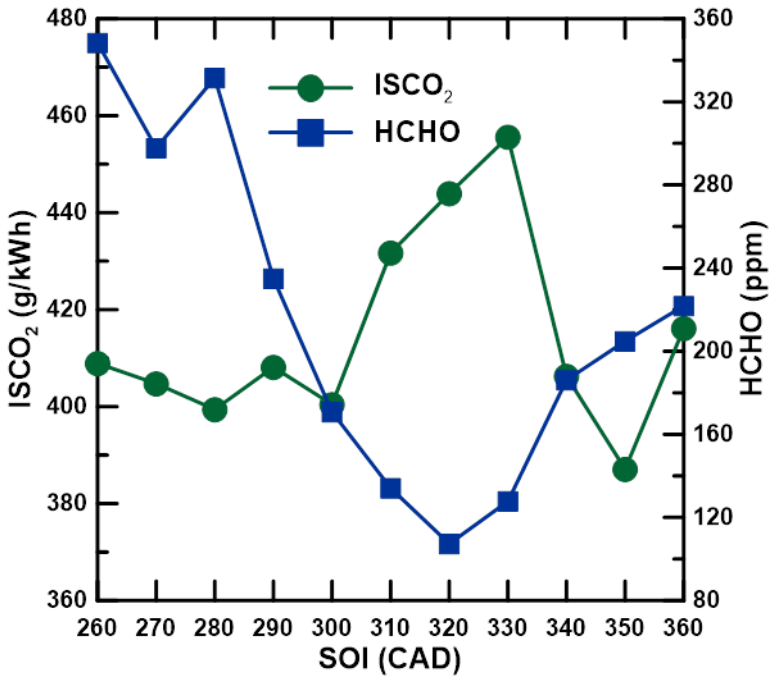

Figure 3.10 $ISCO_2$ and HCHO emissions at various SOIs at 4.1 bar IMEP, 80 PES, N=1500 rev/min, P_{in}=1.5 bar

Figure 3.11 shows the effect of SOI on PM number concentration and size distribution. As SOI is advanced from 350º to 310º, the nanoparticle concentration decreases. As SOI is advanced from 350º to 260º, the diesel pilot spray is injected into a methane-air mixture that is cooler and less dense than that of a more retarded SOI. Therefore, the spray likely penetrates farther into the combustion chamber and mixes more completely with the methane-air mixture causing a decrease in particle concentrations. However, as SOI is advanced to 290º and beyond, PM emissions exhibit a slight increase in particle concentrations. This may be attributed to possible impingement of the diesel spray on the cylinder wall for very advanced SOI, causing locally fuel-rich regions and higher particle concentrations, despite the smoke emissions remaining very low.

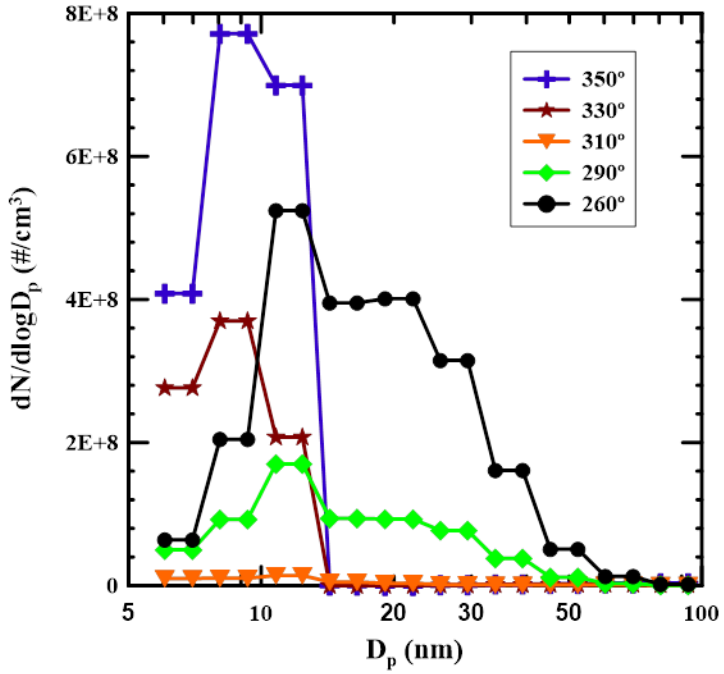

Figure 3.11 PM number concentration and size distribution at various SOIs at 4.1 bar IMEP, 80 PES, N=1500 rev/min, P_{in}=1.5 bar

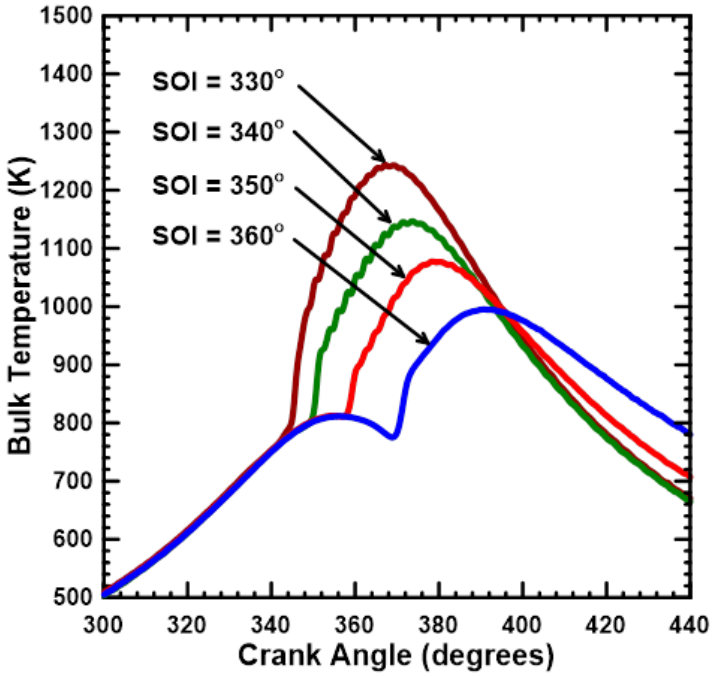

(a)

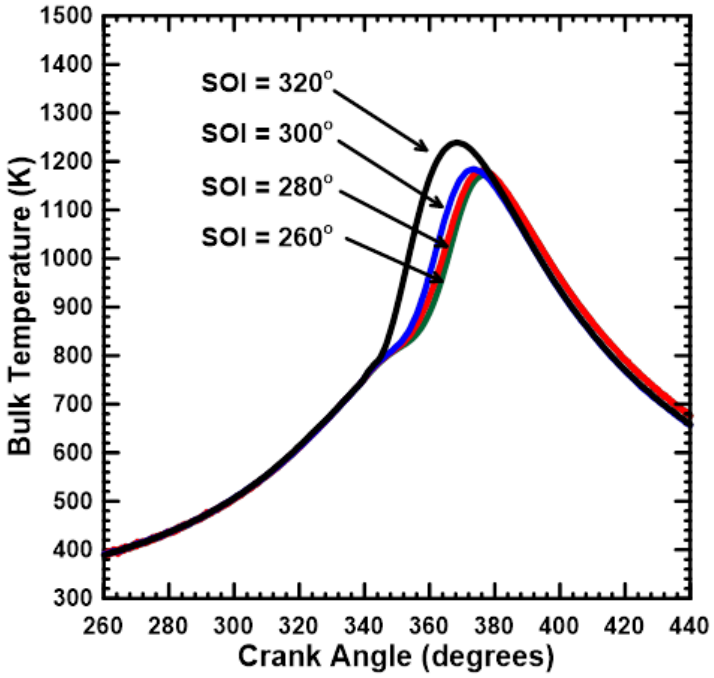

(b)

Figure 3.12 Bulk temperature schedules at (a) late SOIs and (b) advanced SOIs at 4.1 bar IMEP, 80 PES, N=1500 rev/min, P_{in}=1.5 bar

3.2 6.5 bar IMEP: Performance and Emissions

The engine was operated at 6.5 bar IMEP, 1500 rev/min and 80 PES while diesel pilot SOI was varied from 260º to 360º. The diesel injection pressure and intake boost pressure were maintained at 500 bar and 1.5 bar, respectively, and no EGR was used.

3.2.1 Apparent Heat Release Rate and Cylinder Pressure

Figures 3.13 and 3.14 show the cylinder pressure and AHRR histories at various SOIs. Again, a significant change in the shape of the AHRR curve is observed as SOI is advanced from 330º to 320º. For SOI between 360º and 330º, the AHRR curves exhibit two distinct stages of heat release and no significant LTHR peak. The absence of LTHR at retarded SOIs may again be attributed to inhibition of LTHR by relatively higher in-cylinder bulk temperatures at SOI. At these SOIs diesel is injected at relatively higher in-cylinder temperatures of around 800 K as shown in Figure 3.24 (a).

As SOI is advanced earlier in the compression stroke, the separation between EOI and SOC becomes greater. At 320º SOI, fuel injection ends at 330º and the main combustion event starts at 344º which corresponds to approximately 14 CAD difference between SOC and EOI. As the SOI is advanced to 300º, LTHR is still present as the separation increases from 14 CAD to approximately 48 CAD.

As SOI is advanced further from 300º to 260º, the magnitude of heat release increases and the peak heat release is phased after TDC. Again, a decrease in the magnitude of LTHR is observed as SOI is advanced. Compared to lower IMEP results, the LTHR magnitude is lower. This may be attributed to higher in-cylinder bulk temperatures characteristic of higher IMEP, which would suppress LTHR.

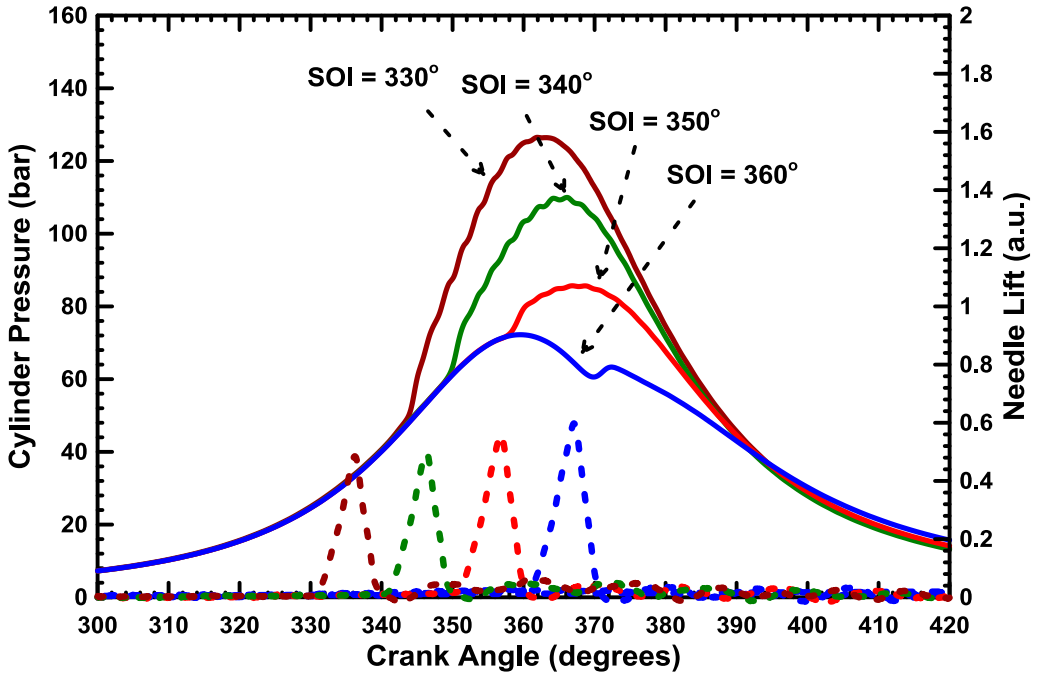

(a)

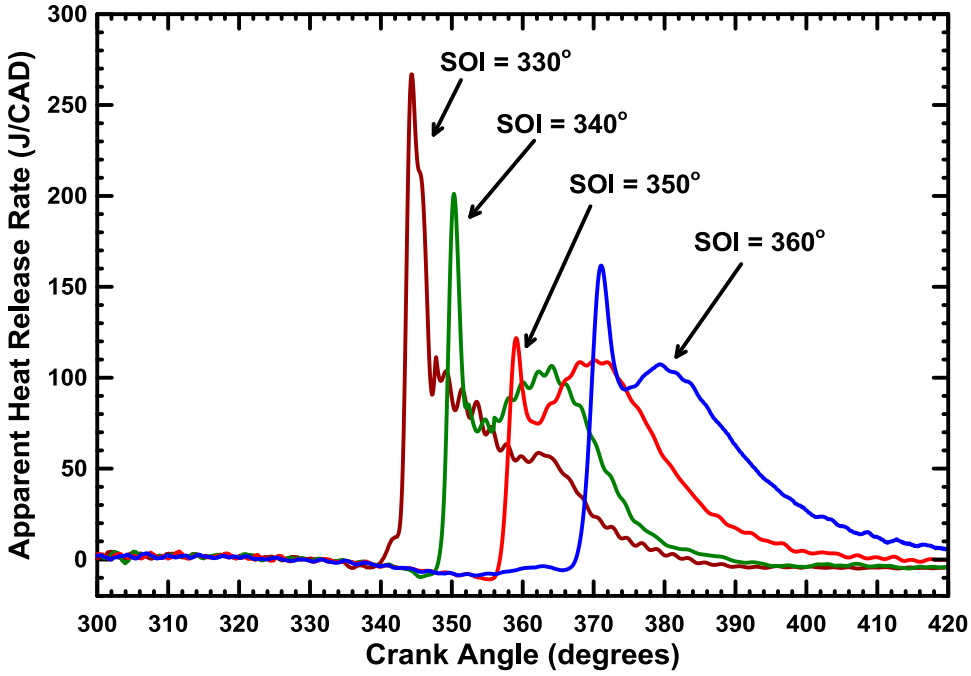

(b)

Figure 3.13 (a) Cylinder pressure histories and (b) crank angle-resolved heat release rates at late SOI at 6.5 bar IMEP, 80 PES, N=1500 rev/min, P_{in}=1.5 bar

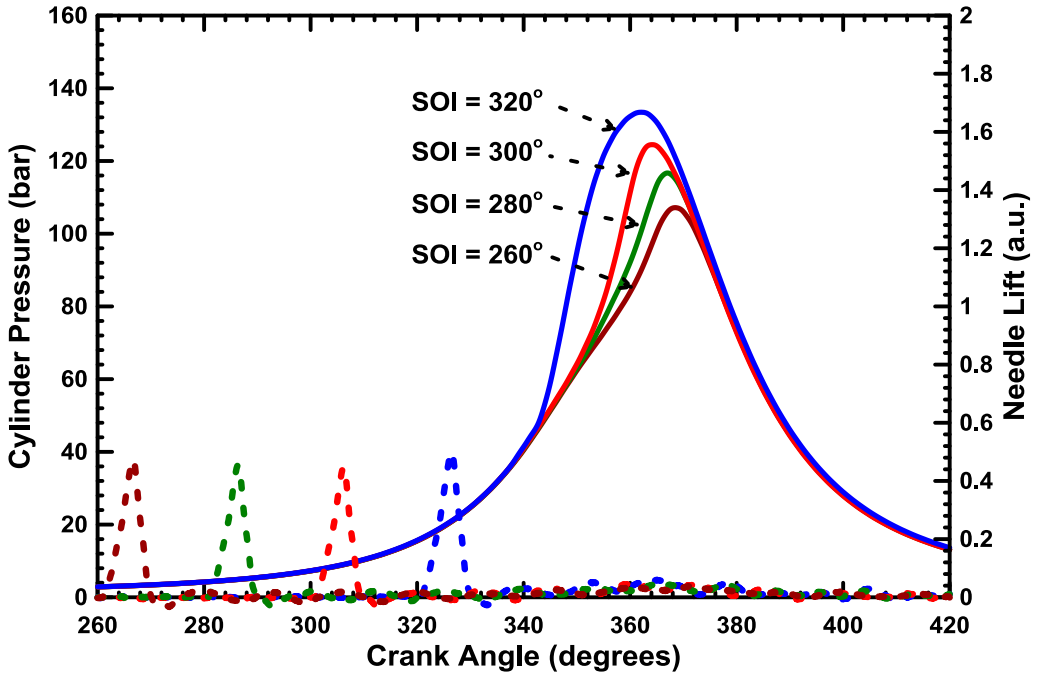

(a)

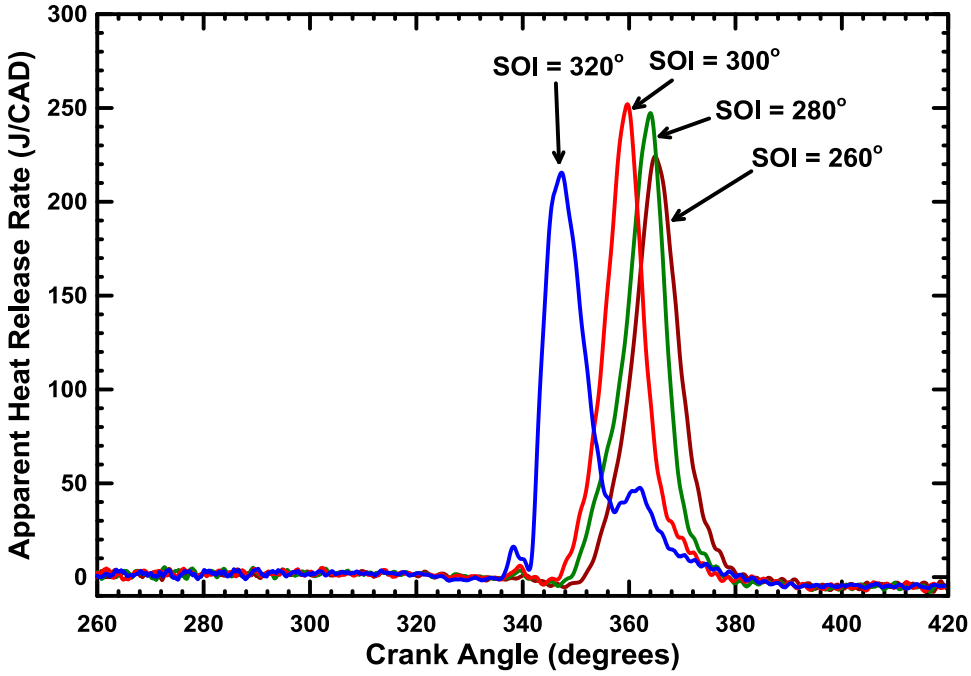

(b)

Figure 3.14 (a) Cylinder pressure histories and (b) crank angle-resolved heat release rates at early SOI at 6.5 bar IMEP, 80 PES, N=1500 rev/min, P_{in}=1.5 bar

3.2.2 Ignition Delay, Maximum Pressure Rise Rate, and Rate of Combustion

Figure 3.15 shows EOI-SOC and ignition delay and Figure 3.16 shows the COV IMEP and MPRR for each SOI. As SOI is advanced beyond 320º, a slight increase in COV IMEP is observed unlike the sharp increase observed at lower IMEP. This difference may be attributed to the increased amount of diesel injected to achieve higher IMEP. Given the same amount of time for mixing, a greater quantity of diesel will not likely become "too well-mixed" as easily. For SOI in the range of 300º to 340º the highest MPRRs are observed, which correlates with the phasing of combustion close to or before TDC as shown in Figure 3.17. As SOI is advanced beyond 330º, a steady increase in ignition delay is observed. This trend may be attributed to decreasing in-cylinder bulk gas temperatures at SOI which would allow for increasingly premixed conditions.

Figure 3.17 shows the CA5, CA50, and CA10-90 for each SOI. A decrease in CA10-90 is observed from about 27 degrees to about 10 degrees when SOI is advanced from 360º to 300º and then remains between 10 and 12 degrees for SOI between 290º and 260º. A relatively consistent CA 10-90 at advanced SOIs might be attributed to "well-mixed", "HCCI-like" combustion. CA50 shifts from after TDC to before TDC when SOI is advanced from 360º to 330º and then shifts back after TDC as SOI is advanced further. This combustion phasing trend likely leads to high MPRR as shown in Figure 3.16 at those conditions. At SOI more advanced than 320º, combustion becomes more "homogeneous" and starts closer to TDC leading to relatively lower MPRR.

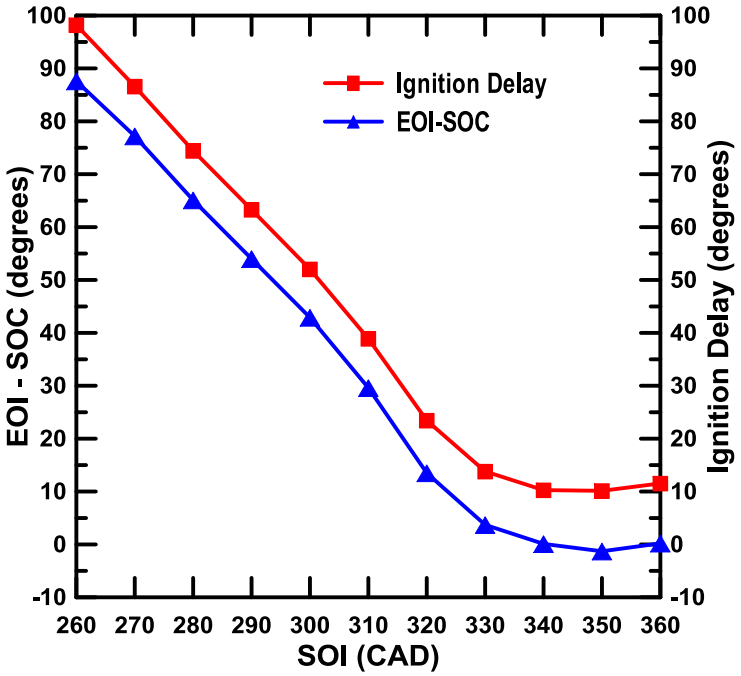

Figure 3.15 EOI-SOC and Ignition delay at various SOIs at 6.5 bar IMEP, 80 PES, N=1500 rev/min, P_{in}=1.5 bar

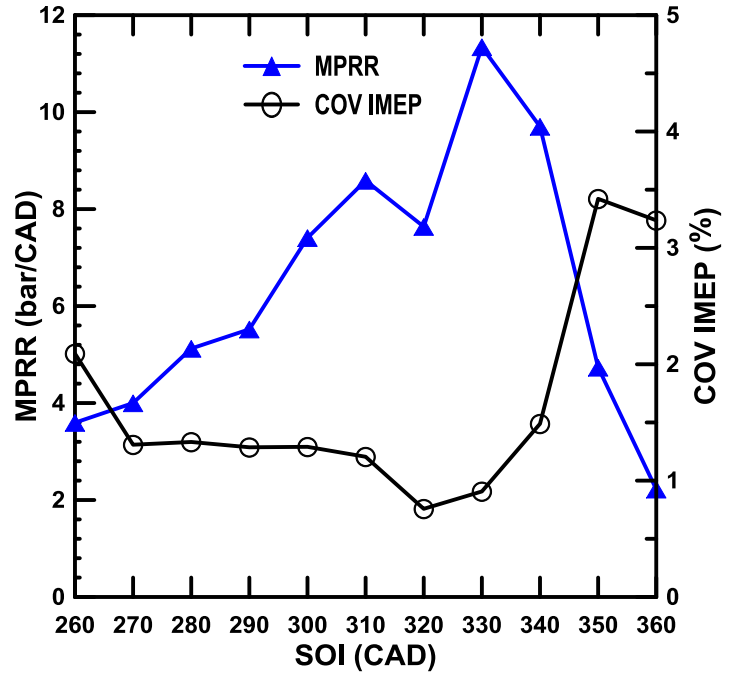

Figure 3.16 COV IMEP and MPRR at various SOIs at 6.5 bar IMEP, 80 PES, N=1500 rev/min, P_{in}=1.5 bar

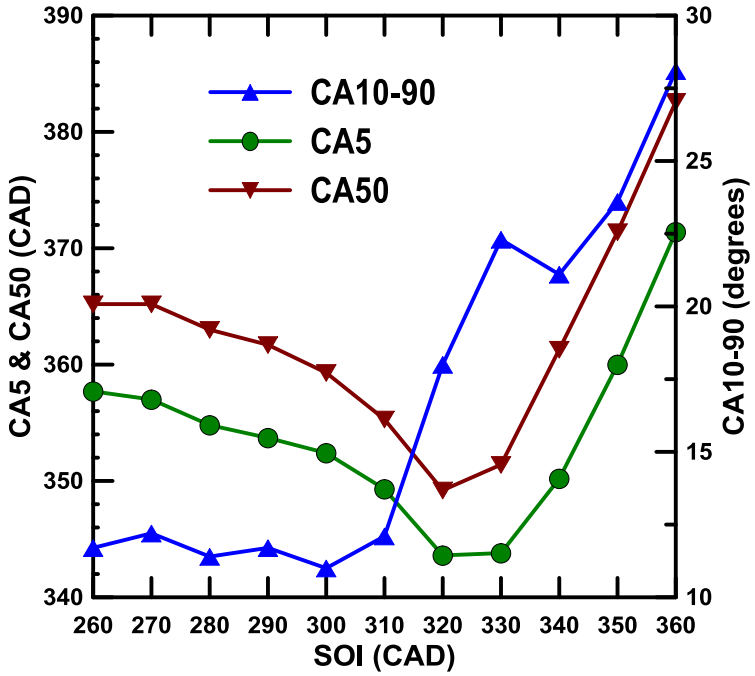

Figure 3.17 CA5, CA50 and CA10-90 at various SOIs at 6.5 bar IMEP, 80 PES, N=1500 rev/min, P_{in}=1.5 bar

3.2.3 Fuel Conversion Efficiency and Combustion Efficiency

Figure 3.18 shows IFCE and combustion efficiency between 360º and 260º SOI. Combustion efficiency decreases as SOI is advanced from 360º to 350º, then increases and reaches a peak value of about 91.5 percent at 320º SOI. Again, an increase in combustion efficiency at advanced SOIs could be attributed to increasingly "well-mixed" conditions. An increase in IFCE is observed from about 29 percent at 360º SOI to about 43.5 percent at 290º SOI followed by a slight decrease in IFCE as SOI is advanced further. This increase in IFCE may be attributed to the increased combustion efficiency at advanced SOI as well as the phasing of CA50 very close to TDC. As SOI is advanced from 290º to 260º a slight decrease in combustion efficiency and IFCE is observed, which may be attributed to the CA50 moving away from TDC.

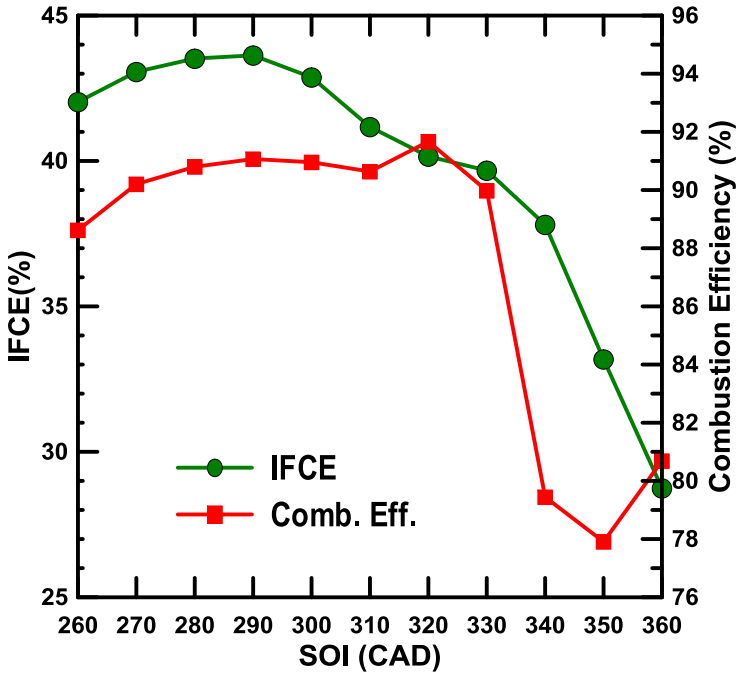

Figure 3.18 Combustion and indicated fuel conversion efficiencies at various SOIs at 6.5 bar IMEP, 80 PES, N=1500 rev/min, P_{in}=1.5 bar

3.2.4 Emissions

Figure 3.20 shows $ISNO_x$ and smoke trends for various SOIs. As SOI is advanced from 360º to 330º, the $ISNO_x$ emissions steeply increase from about 3.5 g/kWh to about 20 g/kWh. However, when SOI is advanced further, the $ISNO_x$ values significantly decrease to around 0.15 g/kWh near 300º SOI and remain low until 260º SOI. Smoke emissions are less than 0.05 FSN for the duration of the SOI sweep. This may be attributed to lean combustion conditions and a high percentage of methane energy substitution. Equivalence ratios for methane-air and diesel-methane-air mixtures at each SOI are shown in Figure 3.19. The very low $ISNO_x$ levels at sufficiently early SOIs is a consequence of increased residence time for mixing of diesel fuel with the lean premixed methane-air mixture. As more time for mixing is allowed, the in-cylinder fuel-air

mixture becomes increasingly homogeneous, which may lead to lower local temperatures.

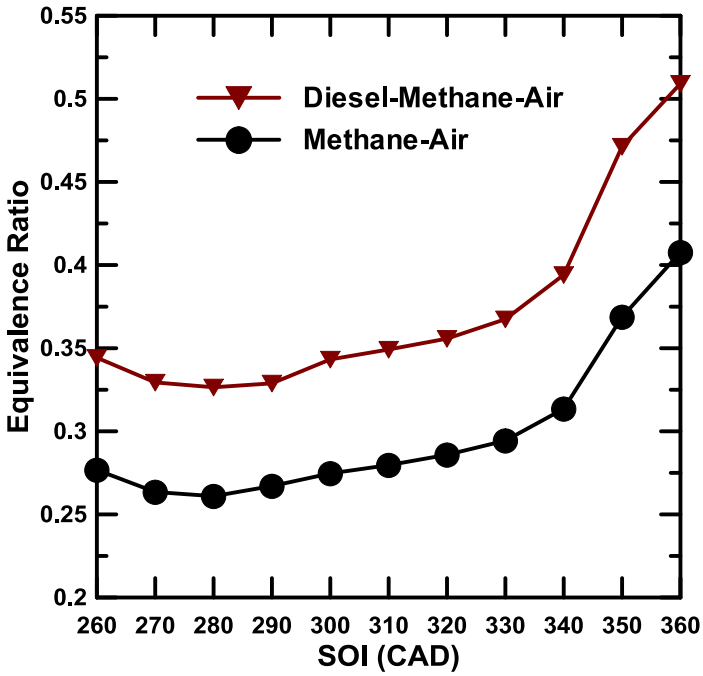

Figure 3.19 Equivalence ratio for methane-air and diesel-methane-air mixtures at various SOIs at 6.5 bar IMEP, 80 PES, N=1500 rev/min, P_{in}=1.5 bar

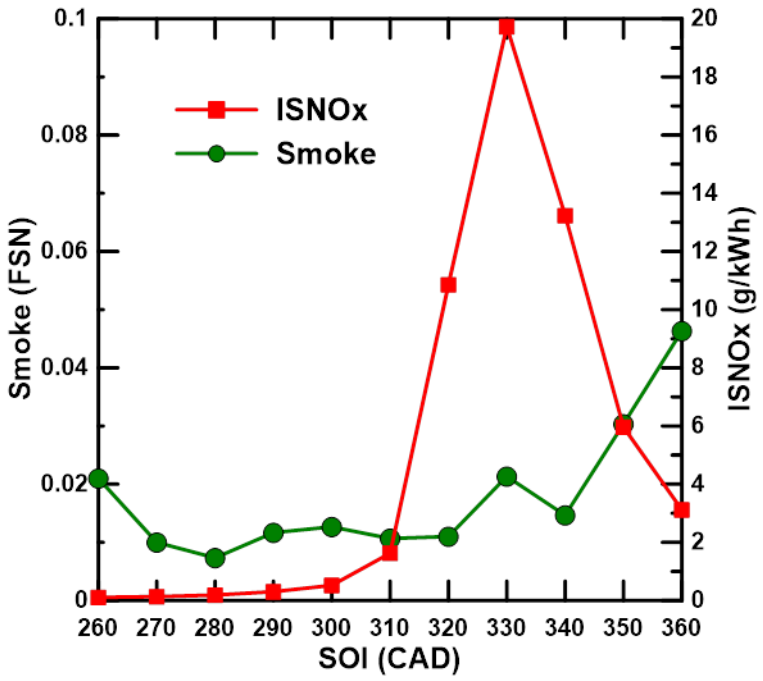

Figure 3.20 $ISNO_x$ and smoke emissions at various SOIs at 6.5 bar IMEP, 80 PES, N=1500 rev/min, P_{in}=1.5 bar

Figure 3.21 shows the ISHC and ISCO emissions and Figure 3.22 shows $ISCO_2$ and HCHO trends between 360º and 260º SOI. A decrease in ISCO emissions is observed from about 20 g/kWh at 360º to 3 g/kWh at 320º followed by an increase to 8 g/kWh at 260º. A decrease in ISHC emissions is observed from 57 g/kWh at 360º to about 15 g/kWh at 320º followed by an increase to about 20 g/kWh at 260º. Both ISHC and ISCO magnitudes are significantly lower at all SOIs compared to lower IMEP results, which may be attributed to higher in-cylinder bulk temperatures characteristic of higher IMEP. Again, the percentage of methane present in the total HC emissions was extremely high for all SOI. However, the actual percentage cannot be quantified from the data collected because it is beyond the scale range of the AVL FTIR analyzer.

As mentioned earlier, temperature significantly influences the rate of HC and CO oxidation. At retarded SOIs between 360º and 350º, peak in-cylinder bulk temperatures are relatively lower, which would inhibit HC and CO oxidation. Again, major sources of unburned hydrocarbons are crevices. At more retarded SOI CA50 is phased well after TDC, so crevice hydrocarbons are not oxidized manifesting in increased ISHC emissions. As SOI is advanced between 330º and 300º, SOC occurs around 350º. The combination of a more advanced SOC as well as increased mixing time available leads to a reduction in ISHC and ISCO emissions. At very advanced SOI between 300º and 260º, ISHC and ISCO emissions exhibit only a slightly increasing trend. This may be attributed to consistently higher in-cylinder bulk temperatures compared to the lower IMEP results, which would continue to promote HC and CO oxidation at advanced SOIs.

For SOIs between 330º and 290º ISCO emissions are fairly low. This may be attributed to the CA50 phased closer to TDC, which could contribute to higher bulk temperatures to support CO oxidation. As SOI is advanced beyond 290º there is only a slight increase in ISCO compared to the sharp increase observed in the 4.1 bar IMEP results. This may be attributed to consistently higher bulk in-cylinder temperatures at advanced SOIs, which would promote increased CO oxidation rates. To support this theory bulk temperature for different SOI are plotted in Figure 3.24. For more retarded SOIs, in-cylinder bulk temperatures during the combustion process are lower than those of SOI between 320º and 260º. For SOIs ranging from 320º to 260º, peak bulk temperatures are 1400 K. Compared to the 4.1 bar IMEP results, the peak temperatures are higher, which could lessen the competition between HC and CO oxidation.

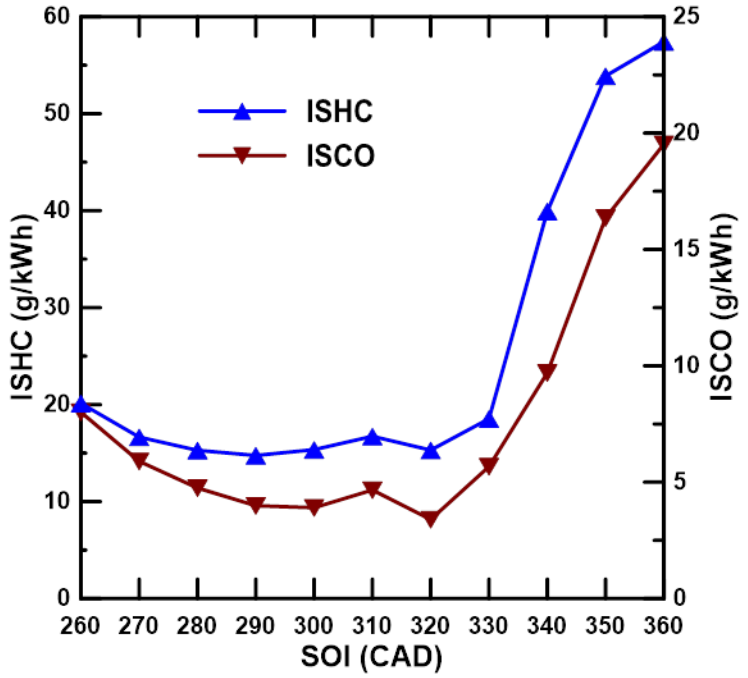

Figure 3.21 ISHC and ISCO emissions at various SOIs at 6.5 bar IMEP, 80 PES, N=1500 rev/min, P_{in}=1.5 bar

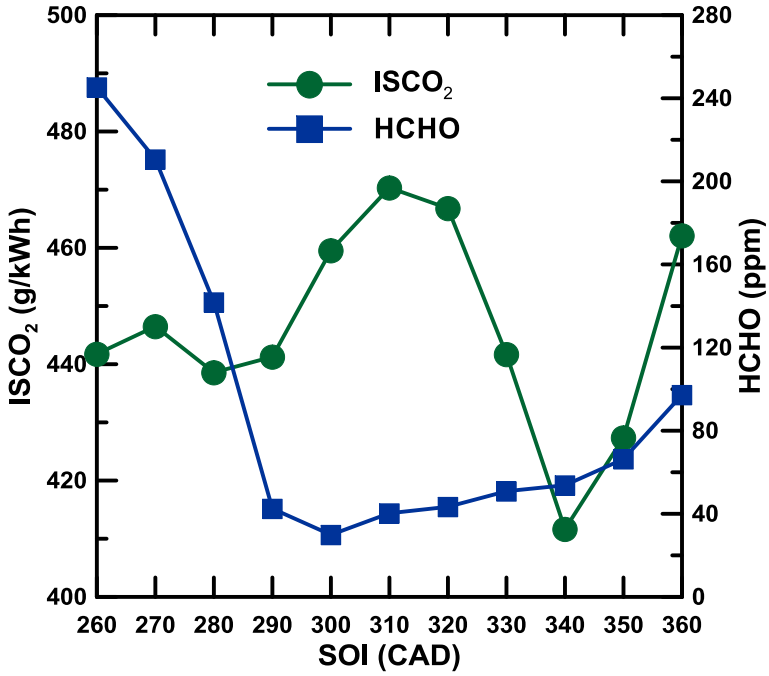

Figure 3.22 $ISCO_2$ and HCHO emissions at various SOIs at 6.5 bar IMEP, 80 PES, N=1500 rev/min, P_{in}=1.5 bar

Figure 3.23 shows the effect of SOI on PM number concentration and size distribution. The magnitude of particle concentrations is higher compared to the lower IMEP results, but the trend is slightly different. No increase in PM concentration is observed when SOI is advanced to 290º and beyond, rather, a monotonic decrease is observed. The reason for this difference in trends is difficult to discern but may be attributed to increased in-cylinder wall temperatures as well as exhaust temperatures at higher IMEP.

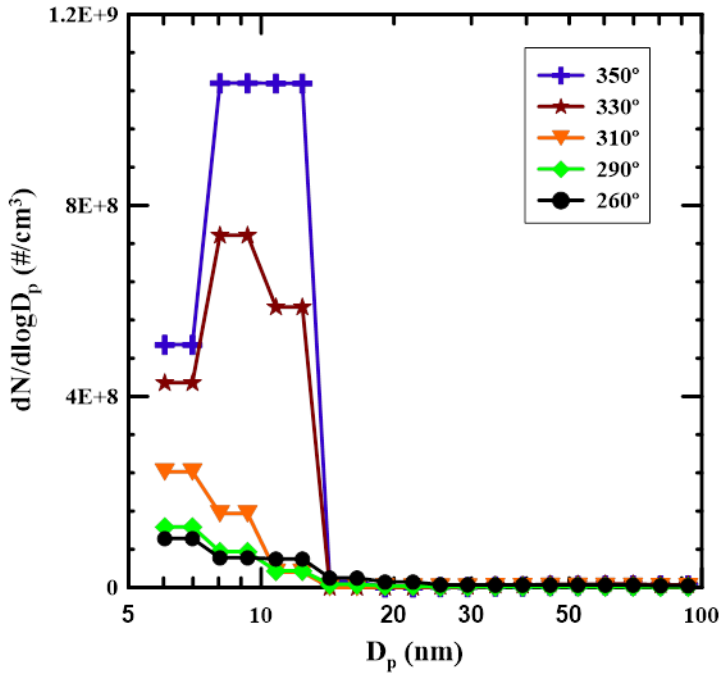

Figure 3.23 PM number concentration and size distribution at various SOIs at 6.5 bar IMEP, 80 PES, N=1500 rev/min, P_{in}=1.5 bar

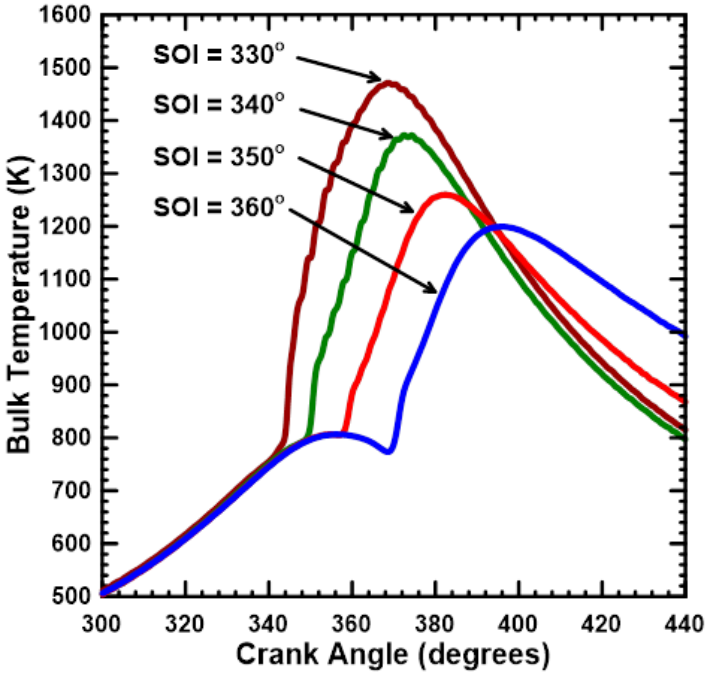

(a)

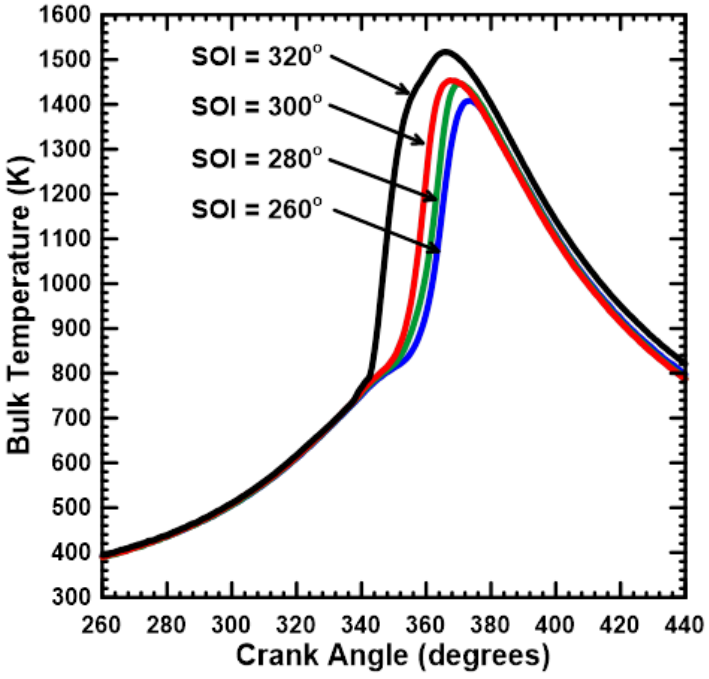

(b)

Figure 3.24 Bulk temperature schedules at (a) late SOIs and (b) advanced SOIs at 6.5 bar IMEP, 80 PES, N=1500 rev/min, P_{in}=1.5 bar

3.3 9.5 bar IMEP: Performance and Emissions

The engine was operated at 9.5 bar IMEP, 1500 rev/min and 88 PES while diesel pilot SOI was varied from 350º to 260º. The diesel injection pressure and intake boost pressure were maintained at 500 bar and 1.8 bar respectively, and no EGR was used. Increased intake pressure was required to avoid high COV IMEP at advanced SOIs. An increase in PES was required to avoid high in-cylinder pressures at advanced SOIs. The SOI sweep was performed at 350º-330º and 310º-260º SOI. The SOI of 360º was omitted due to excessive ISHC emissions while 320º SOI was omitted due to excessive in-cylinder pressure and MPRR.

3.3.1 Apparent Heat Release Rate and Cylinder Pressure

Figures 3.25 and 3.26 show the cylinder pressure and AHRR histories for various SOIs. Again, a significant change in the shape of the AHRR curve is observed as SOI is advanced from 330º to 310º. For SOI between 350º and 330º, the AHRR curves exhibit two distinct stages of heat release and no significant LTHR peak. The absence of LTHR at retarded SOIs may again be attributed to inhibition of LTHR by high in-cylinder bulk temperatures at SOI. At these SOIs diesel is injected at higher in-cylinder temperatures of around 800 K as shown in Figure 3.36 (a).

As SOI is advanced earlier in the compression stroke, the separation between EOI and SOC becomes greater. At 310º, fuel injection ends at 320º and the main combustion event starts at 346º which corresponds to approximately 26 CAD difference between SOC and EOI. As the SOI is advanced to 300º, LTHR is still present as the separation increases from 26 CAD to approximately 41 CAD.

As SOI is advanced further from 310º to 260º, the magnitude of heat release increases and the peak heat release is phased after TDC. Again, a decrease in the magnitude of LTHR is observed as SOI is advanced. Furthermore, compared to lower IMEP results, the magnitude of LTHR is lower. This may again be attributed to higher in-cylinder bulk temperatures characteristic of higher IMEP, which would further suppress LTHR.

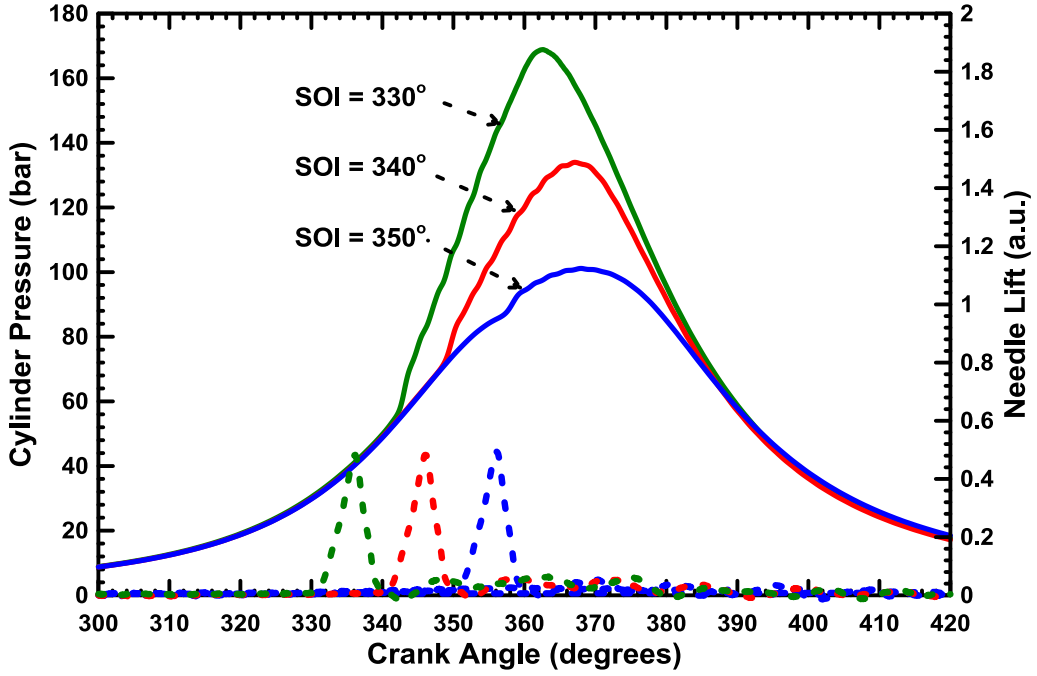

(a)

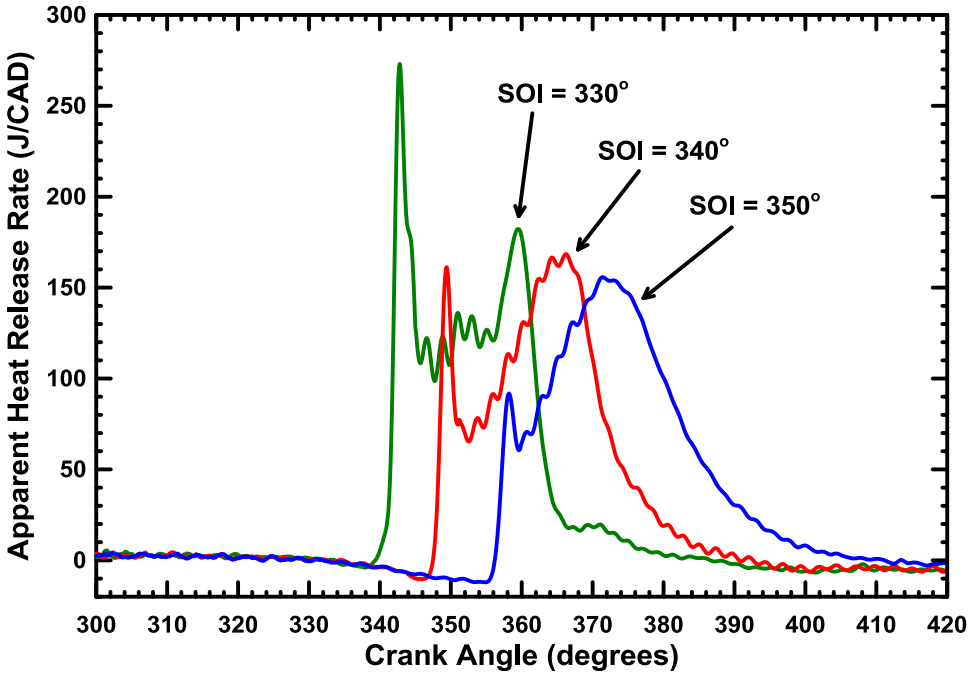

(b)

Figure 3.25 (a) Cylinder pressure histories and (b) crank angle-resolved heat release rates at late SOI at 9.5 bar IMEP, 88 PES, N=1500 rev/min, P_{in}=1.8 bar

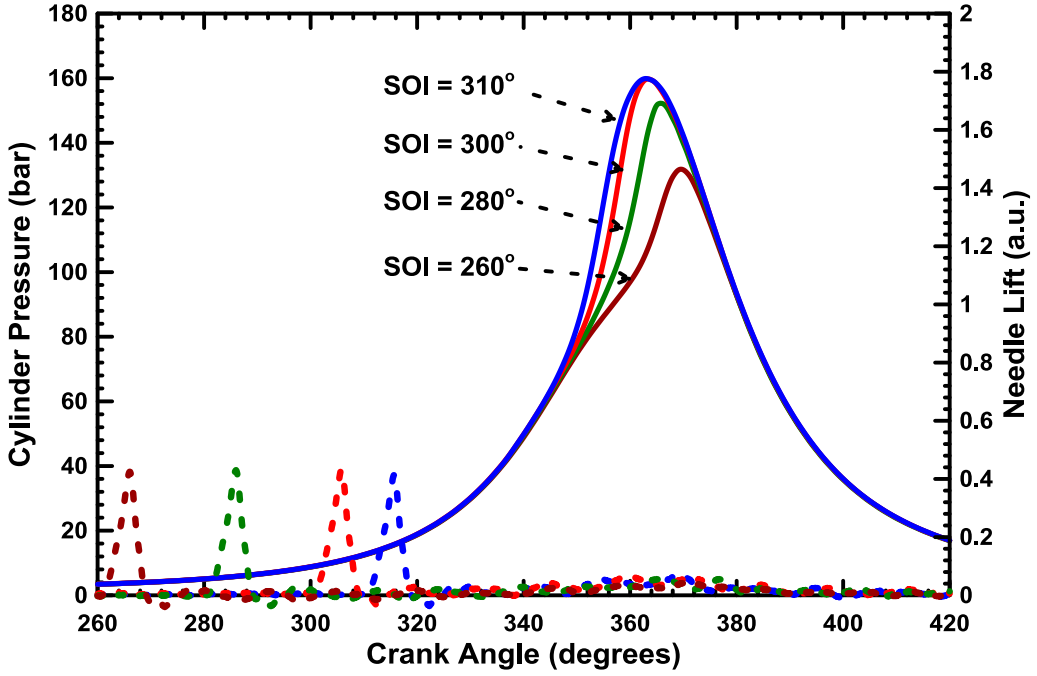

(a)

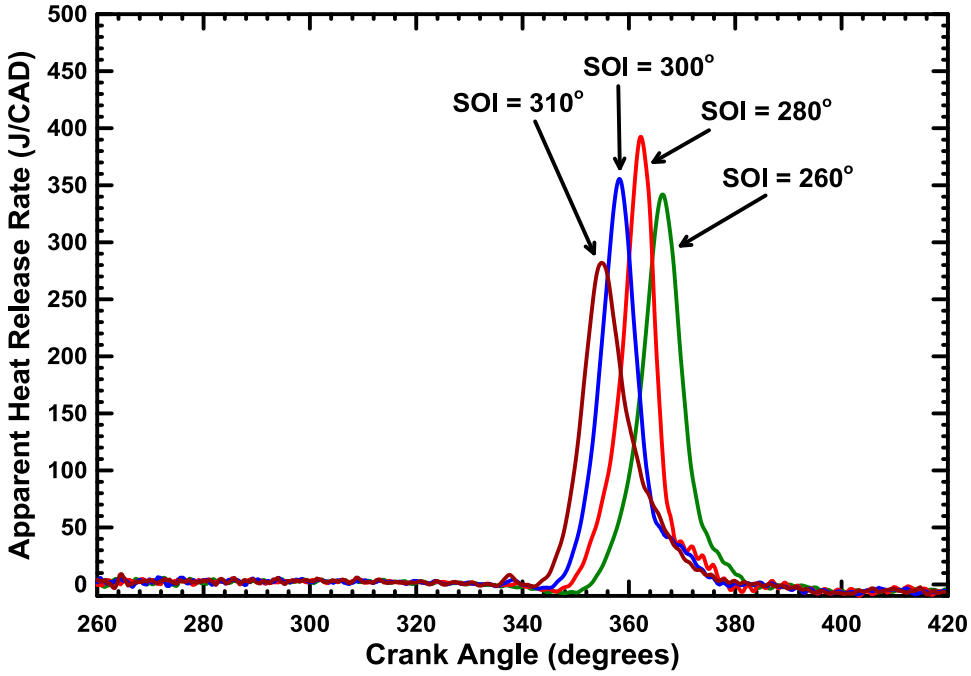

(b)

Figure 3.26 (a) Cylinder pressure histories and (b) crank angle-resolved heat release rates at early SOI at 9.5 bar IMEP, 88 PES, N=1500 rev/min, P_{in}=1.8 bar

3.3.2 Ignition Delay, Maximum Pressure Rise Rate, and Rate of Combustion

Figure 3.27 shows EOI-SOC and ignition delay and Figure 3.28 shows the COV IMEP and MPRR for each SOI. As SOI is advanced beyond 330º, only a slight increase in COV IMEP is observed. This may again be attributed to the increased amount of diesel required to achieve higher IMEP. Although the PES is increased for this SOI sweep, the quantity of diesel may still be sufficient for adequate mixing. For SOIs in the range of 300º to 330º the highest MPRRs are observed. As mentioned earlier, 320º SOI was omitted due to excessive MPRR. Again, as SOI is advanced beyond 330º, a steady increase in ignition delay is observed.

Figure 3.29 shows that CA10-90 decreases from about 23 CAD to about 11 CAD when SOI is advanced from 350º to 300º and then remains between 10 and 11 CAD for SOI between 290º and 260º. A relatively consistent CA10-90 at advanced SOIs might be attributed to "well-mixed", "HCCI-like" combustion. CA50 shifts from after TDC to before TDC when SOI is advanced from 340º to 330º and then shifts back after TDC as SOI is advanced further. This combustion phasing trend likely leads to high MPRR as shown in Figure 3.28 at those conditions. At SOI more advanced than 310º, combustion becomes more "homogeneous" and starts closer to TDC leading to relatively lower MPRR.

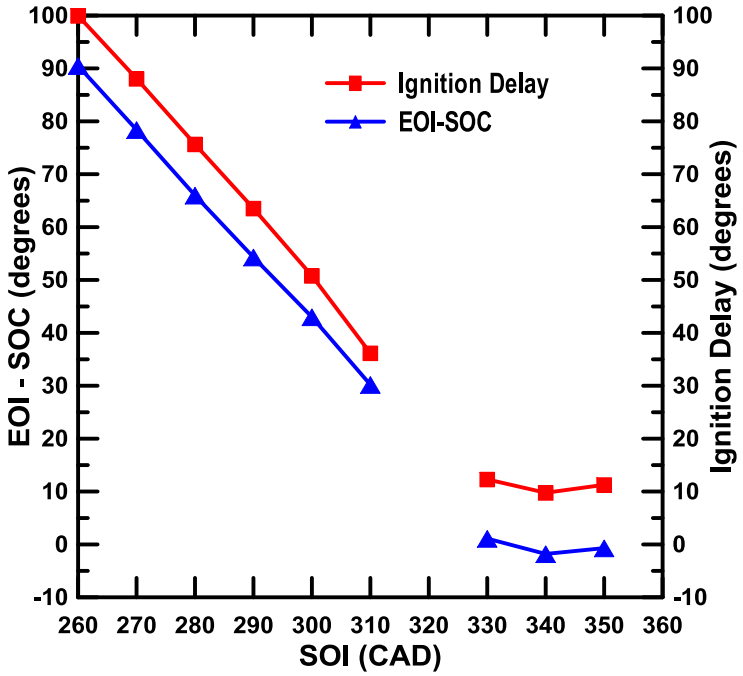

Figure 3.27 EOI-SOC and Ignition delay at various SOIs at 9.5 bar IMEP, 88 PES, N=1500 rev/min, P_{in}=1.8 bar

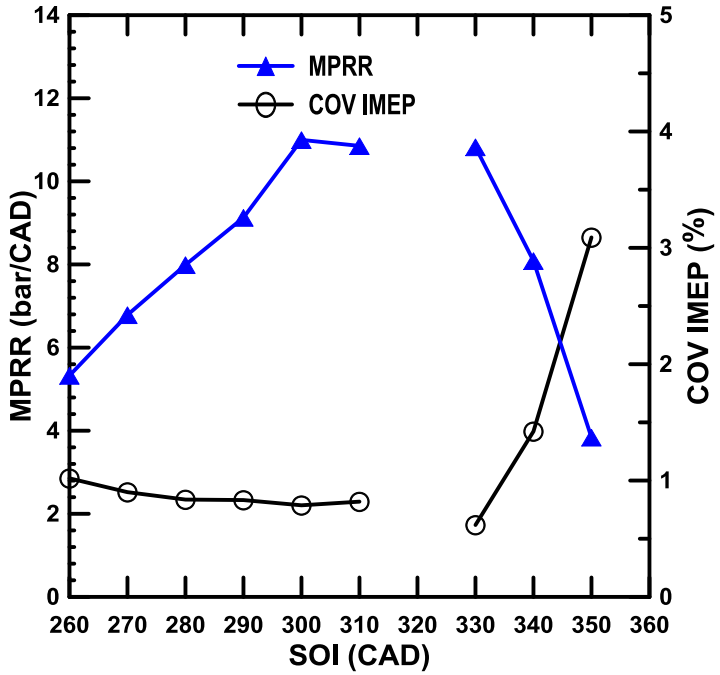

Figure 3.28 COV IMEP and MPRR at various SOIs at 9.5 bar IMEP, 88 PES, N=1500 rev/min, P_{in}=1.8 bar

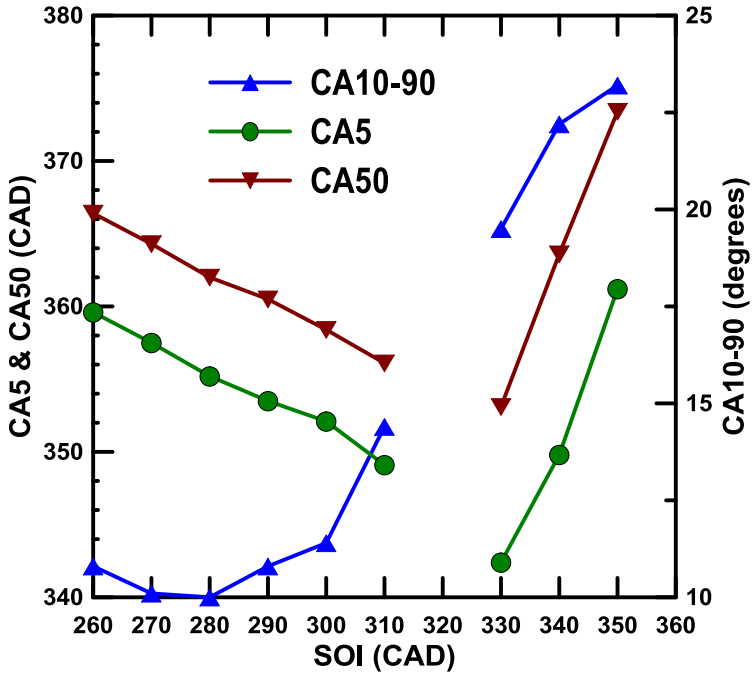

Figure 3.29 CA5, CA50 and CA10-90 at various SOIs at 9.5 bar IMEP, 88 PES, N=1500 rev/min, P_{in}=1.8 bar

3.3.3 Fuel Conversion Efficiency and Combustion Efficiency

Figure 3.30 shows IFCE and combustion efficiency between 350º and 260º SOI. Combustion efficiency decreases as SOI is advanced from 360º to 350º, then increases and reaches a peak value of about 93 percent at 310º SOI. This follows closely with the trend observed during the 6.5 bar IMEP SOI sweep. An increase in IFCE is observed from about 37 percent at 350º SOI to about 46.5 percent at 260º SOI. This increase in IFCE may be attributed to the increased combustion efficiency at advanced SOI as well as the phasing of CA50 closer to TDC.

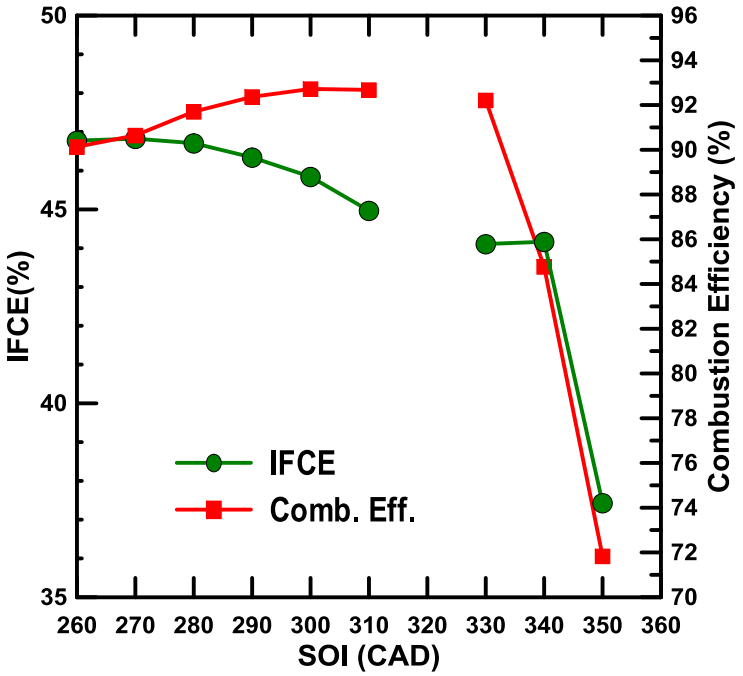

Figure 3.30 Combustion and indicated fuel conversion efficiencies at various SOIs at 9.5 bar IMEP, 88 PES, N=1500 rev/min, P_{in}=1.8 bar

3.3.4 Emissions

Figure 3.32 shows $ISNO_x$ and smoke trends for different SOIs. As SOI is advanced from 350º to 330º, the $ISNO_x$ emissions steeply increase from about 6 g/kWh to about 20 g/kWh. However, when SOI is advanced further, the $ISNO_x$ values significantly decrease to around 0.2 g/kWh and remain low until 260º. Smoke emissions are less than 0.05 FSN for the duration of the SOI sweep. This may be attributed to lean combustion conditions and a high percentage of methane energy substitution. Equivalence ratios for methane-air and diesel-methane-air mixtures at each SOI are shown in Figure 3.31. The very low $ISNO_x$ level at sufficiently early SOIs is a consequence of increased residence time for mixing of diesel fuel with the lean premixed methane-air mixture. As more time for mixing is allowed, the in-cylinder fuel-air mixture becomes increasingly homogeneous, which may lead to lower local temperatures. Although the LTHR magnitudes are relatively low for this load compared to the 6.5 bar IMEP results, the reduced $ISNO_x$ and smoke emissions indicate that LTC conditions may still be present.

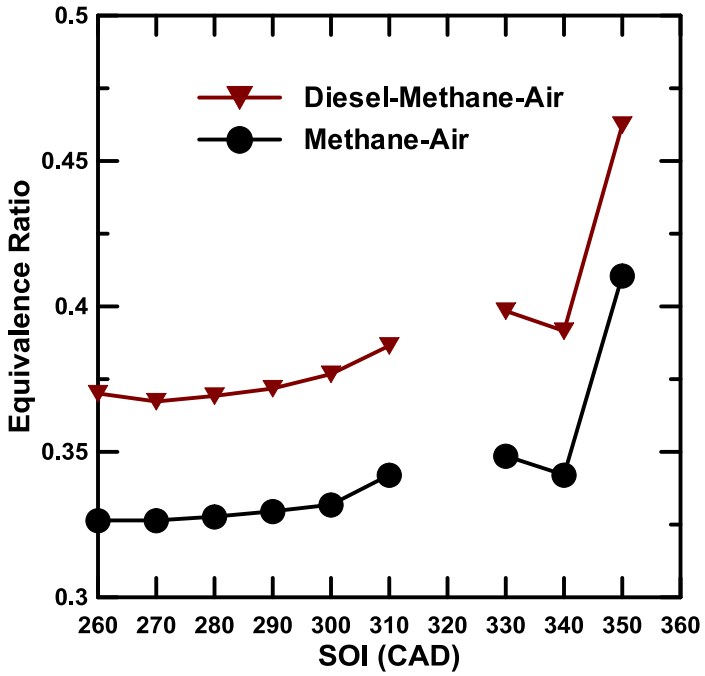

Figure 3.31 Equivalence ratio for methane-air and diesel-methane-air mixtures at various SOIs at 9.5 bar IMEP, 88 PES, N=1500 rev/min, P_{in}=1.8 bar

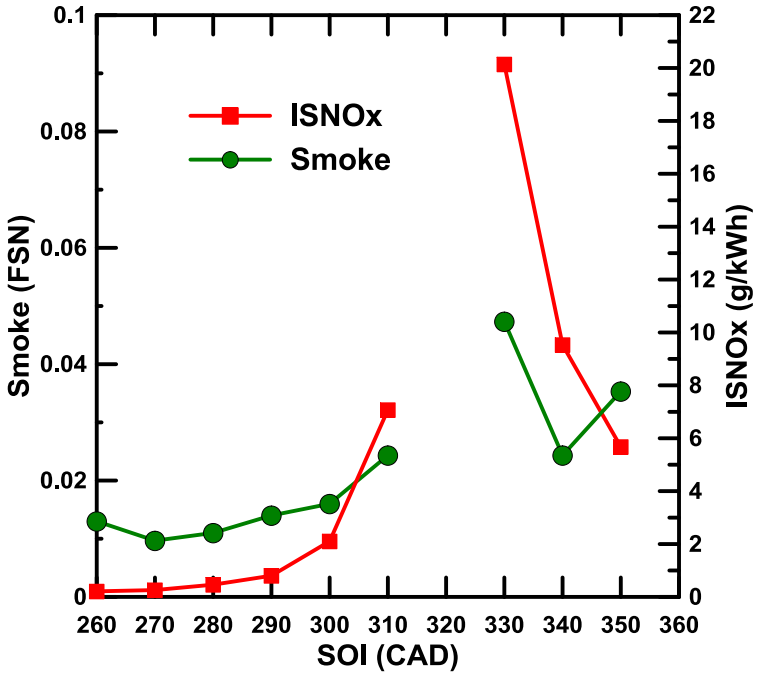

Figure 3.32 $ISNO_x$ and smoke emissions at various SOIs at 9.5 bar IMEP, 88 PES, N=1500 rev/min, P_{in}=1.8 bar

Figure 3.33 shows the ISHC and ISCO and Figure 3.34 shows $ISCO_2$ and HCHO emissions trends between 350º and 260º SOI. A decrease in ISCO emissions is observed from about 8.5 g/kWh at 350º to 1.5 g/kWh at 330º followed by an increase to 3 g/kWh at 260º. A decrease in ISHC emissions is observed from 55 g/kWh at 350º to about 11 g/kWh at 300º followed by an increase to about 15 g/kWh at 260º. Both ISHC and ISCO magnitudes are significantly lower at all SOIs compared to lower IMEP results, which may be attributed to higher in-cylinder bulk temperatures. Again, the percentage of methane present in the total HC emissions was extremely high for all SOI. However, the actual percentage cannot be quantified from the data collected because it is beyond the scale range of the AVL FTIR analyzer.

As mentioned earlier, temperature may have a significant effect on the rate of HC and CO oxidation. At retarded SOIs between 350º and 340º peak in-cylinder bulk temperatures are relatively lower, which would inhibit HC and CO oxidation. Again, major sources of unburned hydrocarbons are crevices. At more retarded SOI CA50 is phased well after TDC, so crevice hydrocarbons are not oxidized manifesting in increased ISHC emissions. As SOI is advanced between 330º and 300º, SOC occurs around 350º. The combination of a more advanced SOC as well as increased mixing time available could lead to a reduction in ISHC and ISCO emissions. At very advanced SOI between 300º and 260º, ISHC and ISCO emissions exhibit a slightly increasing trend. This could be attributed to decreasing combustion duration as illustrated by the CA10-90 trend in Figure 3.29 as well as an increasing COV IMEP as shown in Figure 3.28.

For SOIs between 330º and 290º ISCO emissions are fairly low. This may be attributed to the CA50 phased closer to TDC, which leads to higher bulk temperatures to

support CO oxidation. As SOI is advanced further beyond 290º there is no significant increase in ISCO emissions. This may be attributed to consistently higher bulk in-cylinder temperatures at advanced SOIs, which would promote increased CO oxidation rates. To support this theory bulk temperature for different SOIs are plotted in Figure 3.36. For more retarded SOI, overall bulk temperatures during the combustion process are lower than those of SOI between 330º and 290º. For SOIs ranging from 330º to 260º, peak bulk temperatures are about 1500 K. Compared to the 6.5 bar IMEP results, the peak temperatures are higher, which could increase the rate of HC and CO oxidation.

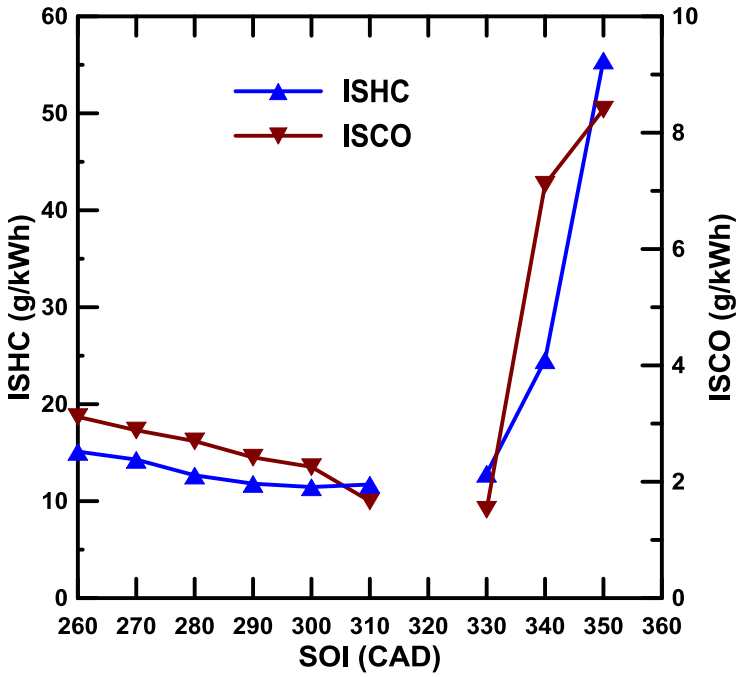

Figure 3.33 ISHC and ISCO emissions at various SOIs at 9.5 bar IMEP, 88 PES, N=1500 rev/min, P_{in}=1.8 bar

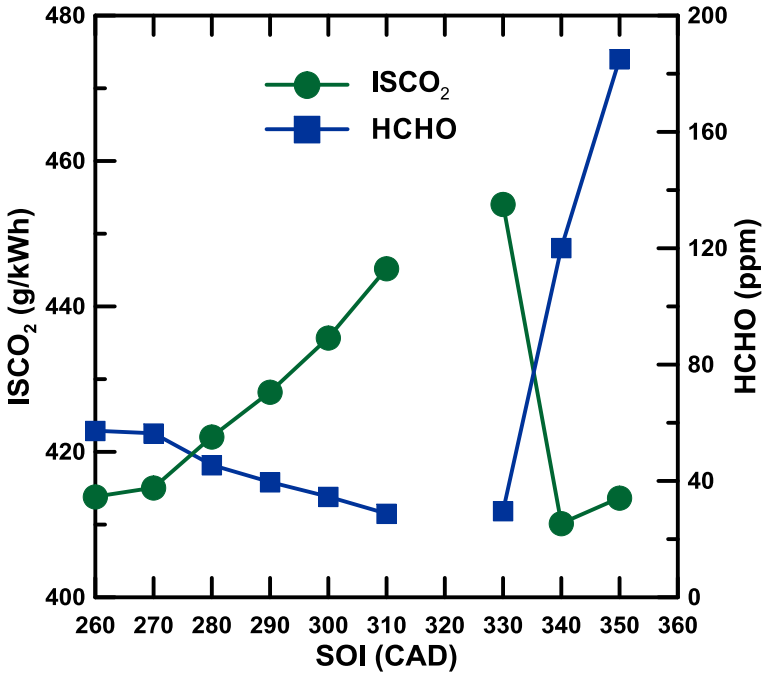

Figure 3.34 $ISCO_2$ and HCHO emissions at various SOIs at 9.5 bar IMEP, 88 PES, N=1500 rev/min, P_{in}=1.8 bar

Figure 3.35 shows the effect of SOI on PM number concentration and size distribution. The magnitude of particle concentrations as well as the trend are highly similar to those observed at 6.5 bar IMEP. No increase in PM concentration is observed when SOI is advanced to 290º and beyond, rather, a monotonic decrease is observed. The reason for this difference in trends is difficult to discern but may be attributed to increased in-cylinder wall temperatures as well as exhaust temperatures at higher IMEP.

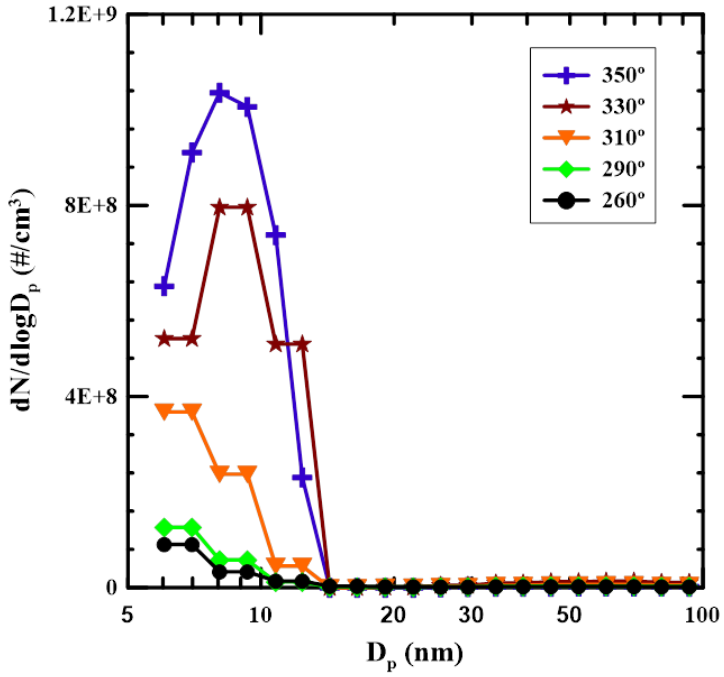

Figure 3.35 PM number concentration and size distribution at various SOIs at 9.5 bar IMEP, 95 PES, N=1500 rev/min, P_{in}=1.8 bar

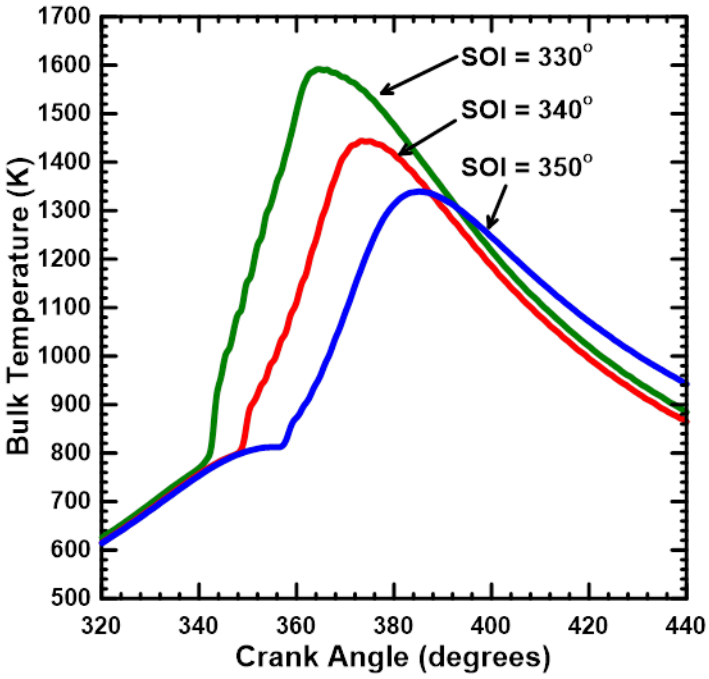

(a)

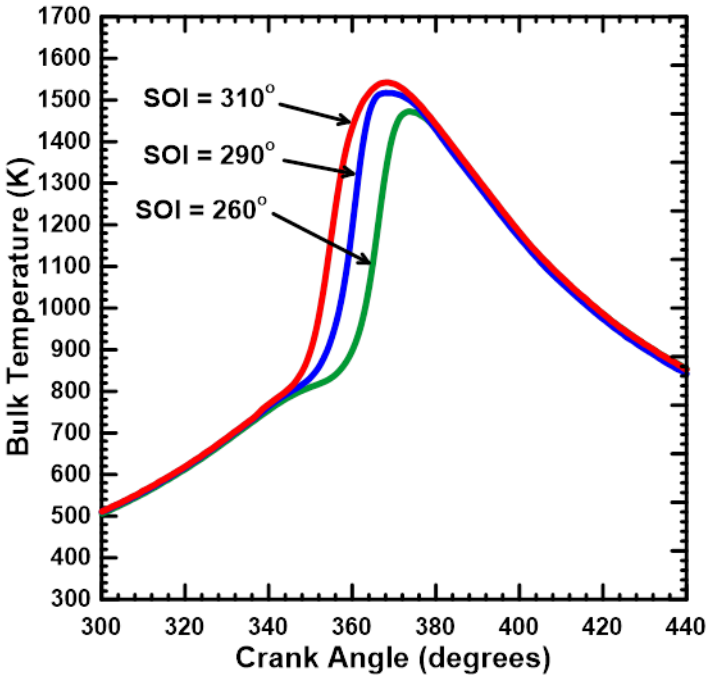

(b)

Figure 3.36 Bulk temperature schedules at (a) late SOIs and (b) advanced SOIs at 9.5 bar IMEP, 88 PES, N=1500 rev/min, P_{in}=1.8 bar

3.4 12.1 bar IMEP: Performance and Emissions

The engine was operated at 12.1 bar IMEP, 1500 rev/min and 95 PES while diesel pilot SOI was varied from 350º to 260º. The diesel injection pressure and intake boost pressure were maintained at 500 bar and 1.8 bar respectively, and no EGR was used. An increase in PES was required to avoid high in-cylinder pressures and MPRRs at advanced SOIs. Furthermore, PES was limited by diesel injection pressure control. These experiments were performed with a standard common-rail diesel injection system. Therefore, it was difficult to maintain constant injection pressures for very small pilot quantities. These experiments were performed at 350º-340º and 310º-260º SOIs. The SOI of 360º was omitted due to excessive ISHC emissions. The SOIs of 330º and 320º were omitted due to excessive in-cylinder pressure and MPRR.

3.4.1 Apparent Heat Release Rate and Cylinder Pressure

Figures 3.37 and 3.38 show the cylinder pressure and AHRR histories for various SOIs. Again, a significant change in the shape of the AHRR curve is observed as SOI is advanced from 340º to 310º. For more retarded SOIs of 350º and 340º, the AHRR curves exhibit two stages of combustion, the majority which occurs in the second stage. This may be attributed to the higher PES setting for this SOI sweep. Furthermore, peak AHRR magnitudes decrease at advanced SOIs. This trend may be attributed to an increasing COV IMEP as illustrated in Figure 3.40. Unlike the lower IMEP AHRR results, there are no indications of LTHR at 12.1 bar IMEP. This may be attributed to significantly higher in-cylinder bulk temperatures, which would prevent LTHR from occurring.

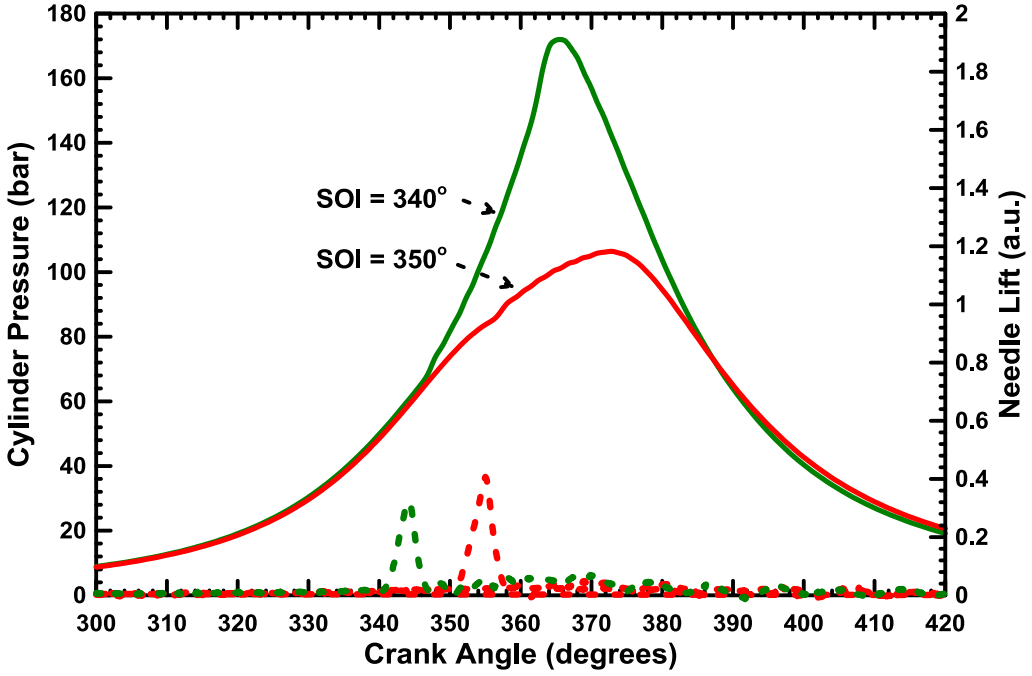

(a)

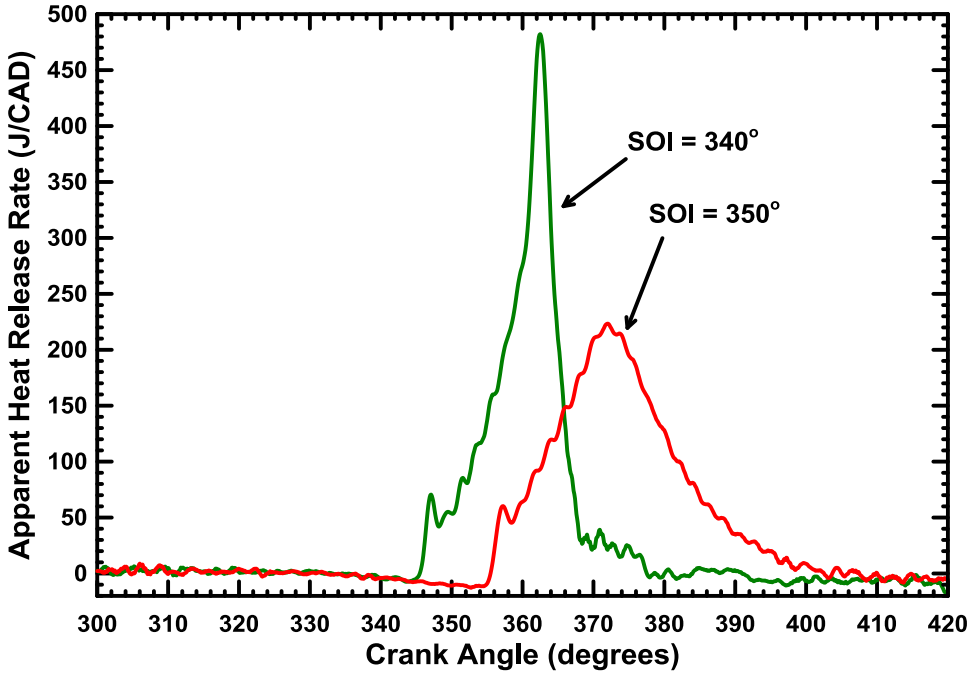

(b)

Figure 3.37 (a) Cylinder pressure histories and (b) crank angle-resolved heat release rates at late SOI at 12.1 bar IMEP, 95 PES, N=1500 rev/min, P_{in}=1.8 bar

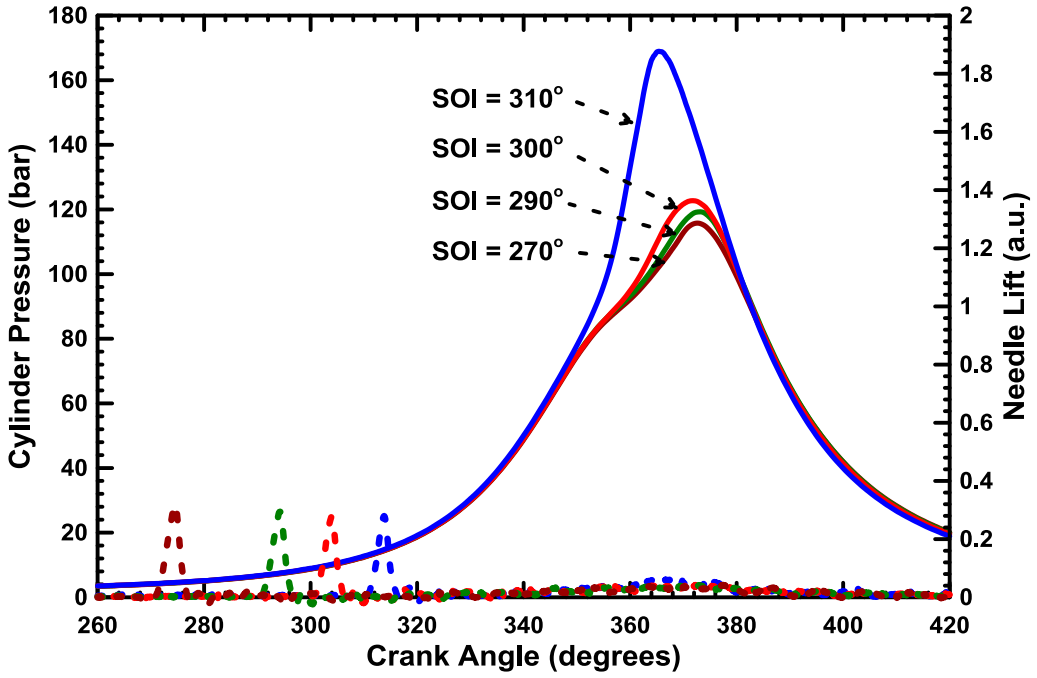

(a)

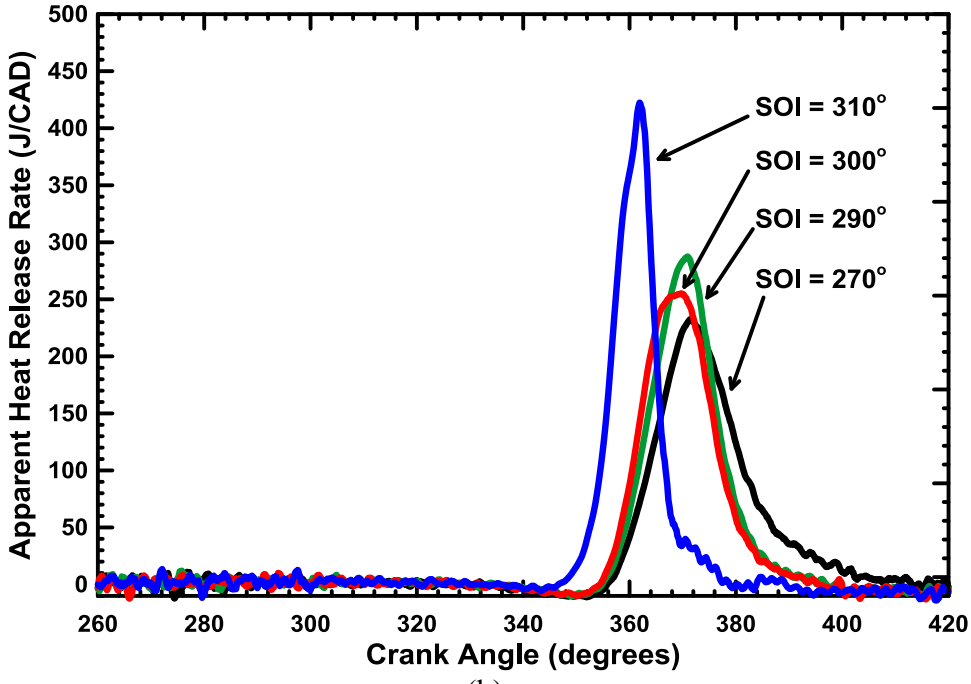

(b)

Figure 3.38 (a) Cylinder pressure histories and (b) crank angle-resolved heat release rates at early SOI at 12.1 bar IMEP, 95 PES, N=1500 rev/min, P_{in}=1.8 bar

3.4.2 Ignition Delay, Maximum Pressure Rise Rate, and Rate of Combustion

Figure 3.39 shows EOI-SOC and ignition delay and Figure 3.40 shows the COV IMEP, MPRR, and ignition delay for each SOI. As SOI is advanced beyond 310º, a sharp increase in COV IMEP is observed. This trend is comparable to the trend observed in the 4.1 bar IMEP results. Since the PES is increased for this SOI sweep, the quantity of diesel required to achieve 12.1 bar IMEP may be small enough to exhibit "too well-mixed" conditions at advanced SOIs. For SOI in the range of 310º to 340º the highest MPRRs are observed. As mentioned earlier, 320º and 330º SOIs were omitted due to excessive in-cylinder pressure and MPRR. Again, as SOI is advanced beyond 340º, a steady increase in ignition delay is observed.

Figure 3.41 shows that CA10-90 decreases from about 23 CAD to about 11 CAD when SOI is advanced from 350º to 310º and then increases to about 20 CAD for 270º SOI. This trend is quite different from the relatively consistent CA10-90 observed at advanced SOIs at lower IMEPs. The increase in CA10-90 at very advanced SOIs may be attributable to the higher PES, which might require more time for flame propagation through the methane-air mixture. CA50 shifts from after TDC to very close to TDC when SOI is advanced from 340º to 310º and then shifts after TDC as SOI is advanced further. This combustion phasing trend likely leads to high MPRR as shown in Figure 3.40 at those conditions. At SOI more advanced than 310º, combustion becomes more "homogeneous" and starts closer to TDC leading to relatively lower MPRR.

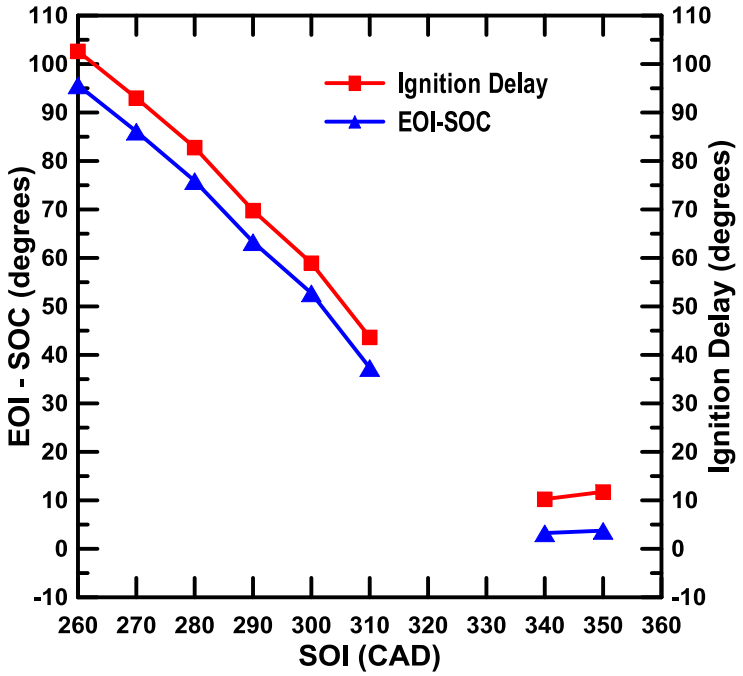

Figure 3.39 EOI-SOC and Ignition delay at various SOIs at 12.1 bar IMEP, 95 PES, N=1500 rev/min, P_{in}=1.8 bar

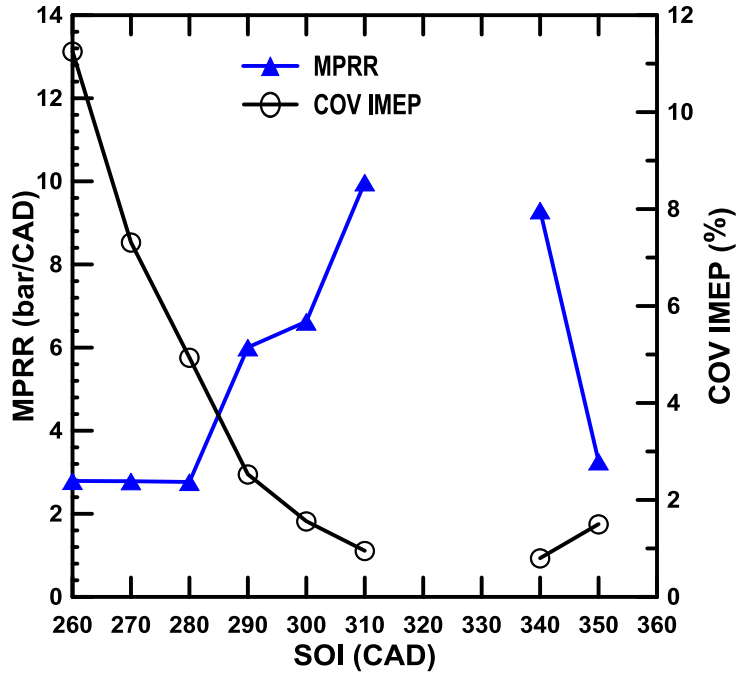

Figure 3.40 COV IMEP and MPRR at various SOIs at 12.1 bar IMEP, 95 PES, N=1500 rev/min, P_{in}=1.8 bar

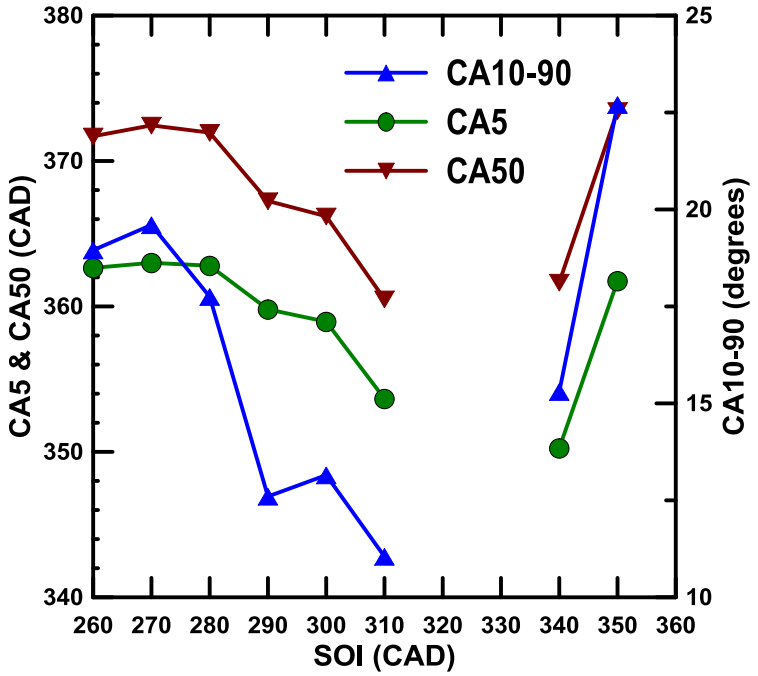

Figure 3.41 CA5, CA50 and CA10-90 at various SOIs at 12.1 bar IMEP, 95 PES, N=1500 rev/min, P_{in}=1.8 bar

3.4.3 Fuel Conversion Efficiency and Combustion Efficiency

Figure 3.42 shows IFCE and combustion efficiency between 350º and 260º SOI. Combustion efficiency increases as SOI is advanced from 350º to 310º reaching a peak value of about 92 percent at 310º SOI. Again, an increase in combustion efficiency at advanced SOIs could be attributed to increasingly "well-mixed" conditions. An increase in IFCE is observed from about 42 percent at 350º SOI to about 44.5 percent at 290º SOI. This increase in IFCE may be attributed to the increased combustion efficiency at advanced SOI as well as the phasing of CA50 closer to TDC. As SOI is advanced from 310º to 260º a decrease in combustion efficiency and IFCE is observed, which may be attributed to the CA50 moving away from TDC as well as the increasing COV IMEP.

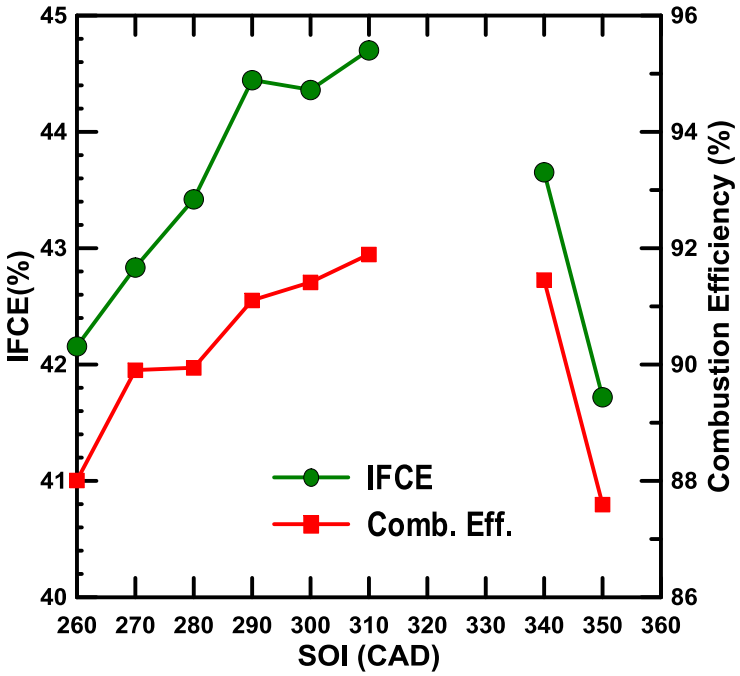

Figure 3.42 Combustion and indicated fuel conversion efficiencies at various SOIs at 12.1 bar IMEP, 95 PES, N=1500 rev/min, P_{in}=1.8 bar

3.4.4 Emissions

Figure 3.44 shows $ISNO_x$ and smoke trends for different SOIs. As SOI is advanced from 350º to 340º, the $ISNO_x$ emissions increase from about 4.6 g/kWh to about 13.6 g/kWh. However, when SOI is advanced further, the $ISNO_x$ values significantly decrease to around 1.3 g/kWh and remain between 1.3 and 1.5 g/kWh until 260º SOI. Smoke emissions are less than 0.05 FSN for the duration of the SOI sweep. This may be attributed to lean combustion conditions and a high percentage of methane energy substitution. Equivalence ratios for methane-air and diesel-methane-air mixtures at each SOI are shown in Figure 3.43.

The decreasing $ISNO_x$ trend as SOI is advanced is a consequence of increasing residence time for mixing of diesel fuel with the lean premixed methane-air. As more time for mixing is allowed, the in-cylinder fuel-air mixture becomes increasingly

homogeneous, which may lead to lower local temperatures. However, a reduction in ISNOx to levels observed at lower IMEPs in this study is not observed at this IMEP. This trend seems counterintuitive but can be explained by equivalence ratios and in-cylinder temperatures at this IMEP. Throughout this SOI sweep, in-cylinder bulk temperatures (shown in Figure 3.48) are much higher compared to those of lower IMEP SOI sweeps. Increased in-cylinder bulk temperatures as well as a higher equivalence ratio (i.e. a more fuel-rich in-cylinder environment) compared to lower IMEP results could be indicative of increased local temperatures, which would prevent the reduction of $ISNO_x$. In this regard, EGR would be helpful in reducing the in-cylinder temperatures.

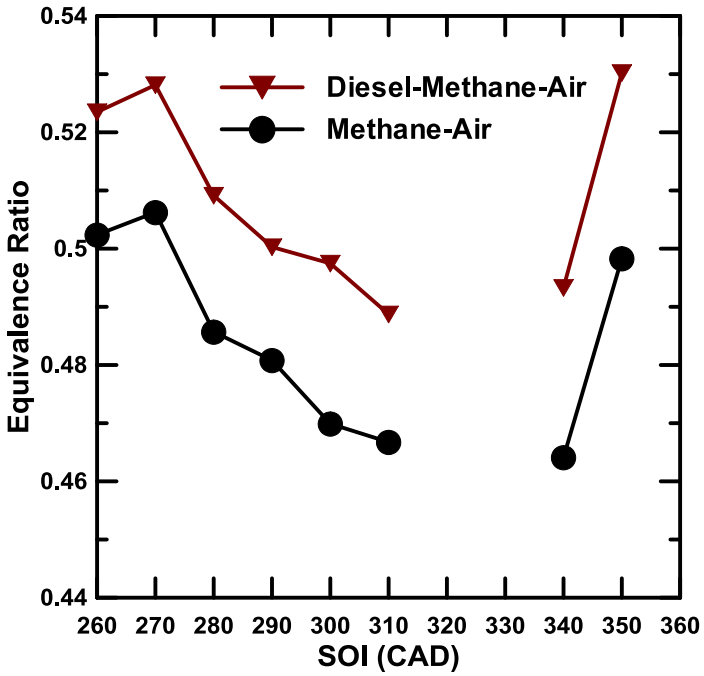

Figure 3.43 Equivalence ratio for methane-air and diesel-methane-air mixtures at various SOIs at 12.1 bar IMEP, 95 PES, N=1500 rev/min, P_{in}=1.8 bar

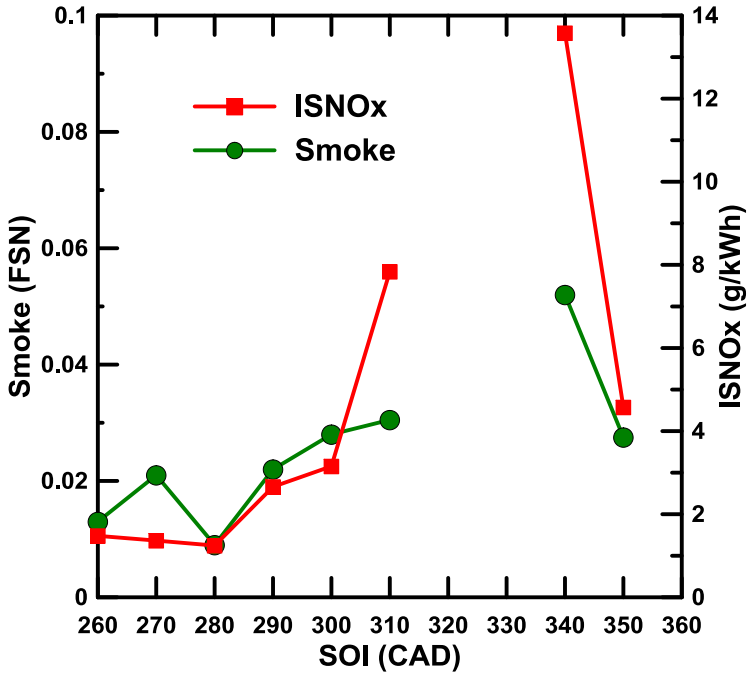

Figure 3.44 $ISNO_x$ and smoke emissions at various SOIs at 12.1 bar IMEP, 95 PES, N=1500 rev/min, P_{in}=1.8 bar

Figure 3.45 shows the ISHC and ISCO and Figure 3.46 shows $ISCO_2$ and HCHO emissions trends between 350º and 260º SOI. A decrease in ISCO emissions is observed from about 5 g/kWh at 350º to 2.5 g/kWh at 310º followed by an increase to 3.5 g/kWh at 260º. A decrease in ISHC emissions is observed from 22 g/kWh at 350º to about 13.4 g/kWh at 310º followed by an increase to about 21 g/kWh at 260º. The percentage of methane present in the total HC emissions was extremely high for all SOI. However, the actual percentage cannot be quantified from the data collected because it is beyond the scale range of the AVL FTIR analyzer.

As mentioned earlier, temperature may have a significant effect on the rate of HC and CO oxidation. For SOIs ranging from 310º to 260º, peak bulk temperatures are around 1600 K. The significantly increased temperatures may promote accelerated HC

and CO oxidation rates and contribute to subtle increases and decreases in ISHC and ISCO emissions. Again, major sources of unburned hydrocarbons are crevices. At SOI close to TDC, CA50 is phased well after TDC, so crevice hydrocarbons are not oxidized manifesting in increased ISHC emissions. As SOI is advanced between 340º and 310º, SOC occurs around 350º. The combination of a more advanced SOC as well as increased mixing time available could lead to a reduction in ISHC and ISCO emissions. At very advanced SOI between 300º and 260º, ISHC and ISCO emissions exhibit a slightly increasing trend. This may be attributed to the increasing COV IMEP as shown in Figure 3.40.

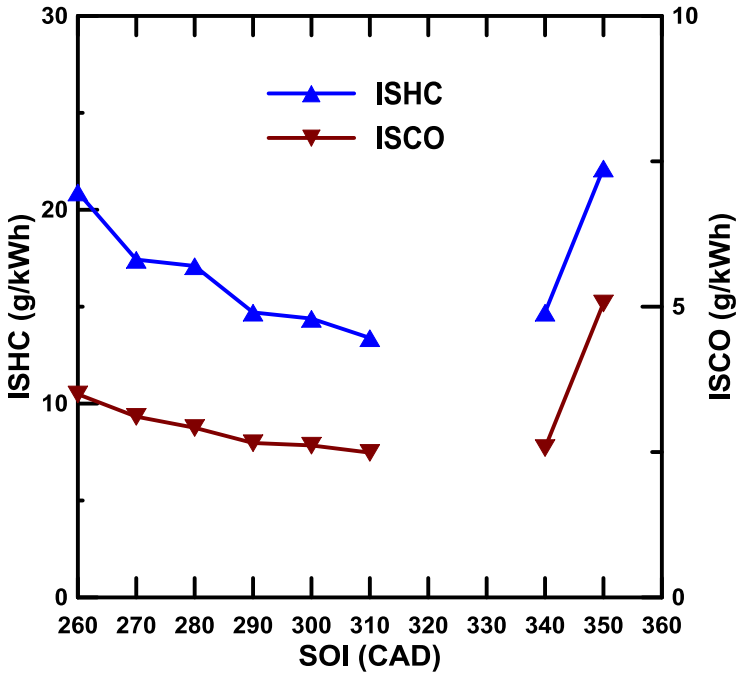

Figure 3.45 ISHC and ISCO emissions at various SOIs at 12.1 bar IMEP, 95 PES, N=1500 rev/min, P_{in}=1.8 bar

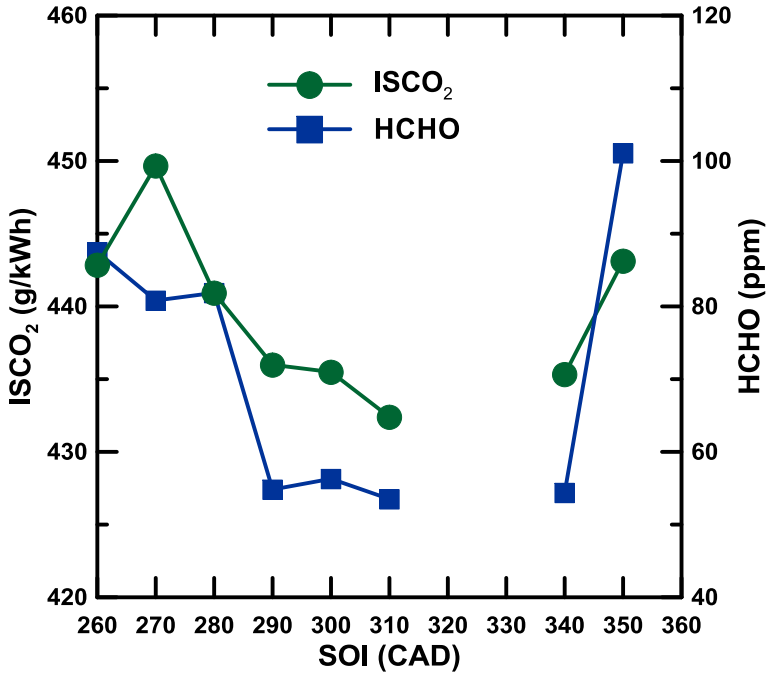

Figure 3.46 $ISCO_2$ and HCHO emissions at various SOIs at 12.1 bar IMEP, 95 PES, N=1500 rev/min, P_{in}=1.8 bar

Figure 3.47 shows the effect of SOI on PM number concentration and size distribution. The trend observed is similar to that of the 4.1 bar IMEP results (i.e. a slight increase in particle concentration is observed when SOI is advanced to 290º and beyond) but the magnitude of particle concentrations is lower. Again, the reason for the differences in particle emissions is difficult to discern but may be attributed to an increased PES, higher in-cylinder wall temperatures, and higher exhaust temperatures at 12.1 bar IMEP.

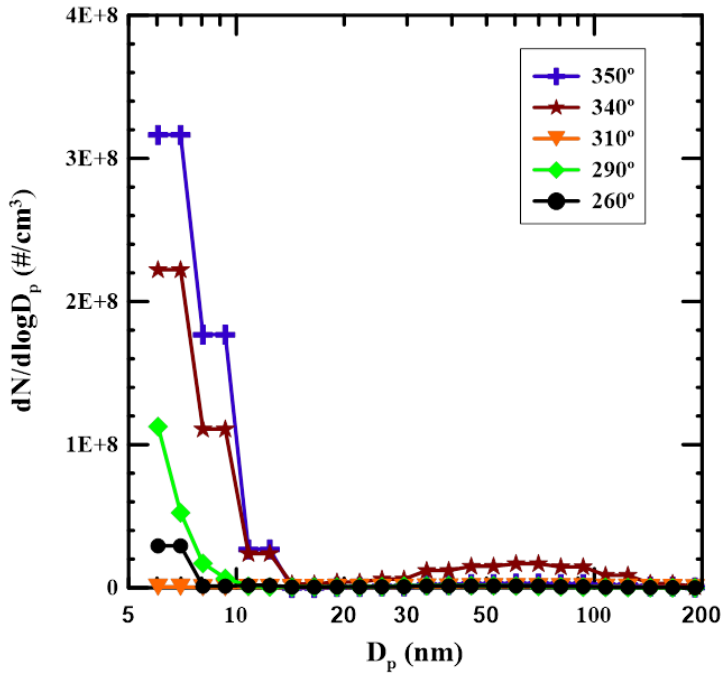

Figure 3.47 PM number concentration and size distribution at various SOIs at 12.1 bar IMEP, 95 PES, N = 1500 rev/min, P_{in} = 1.8 bar

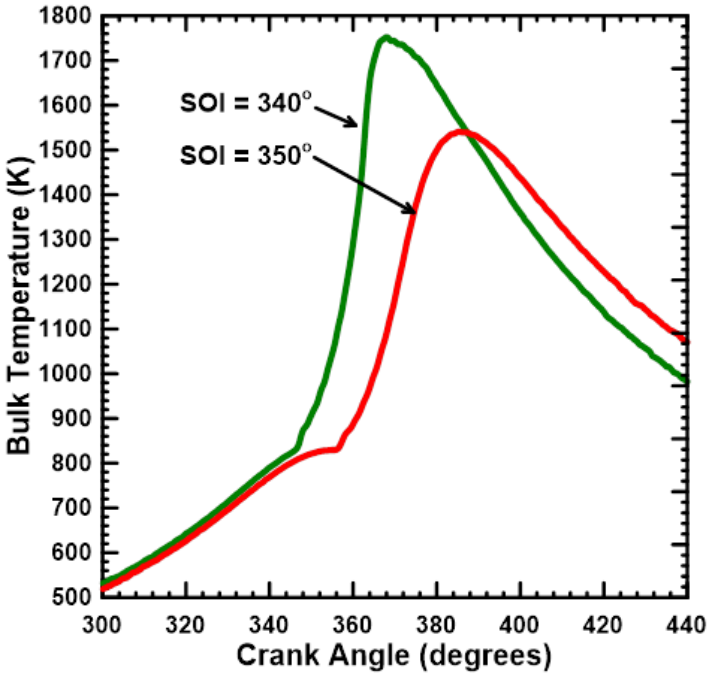

(a)

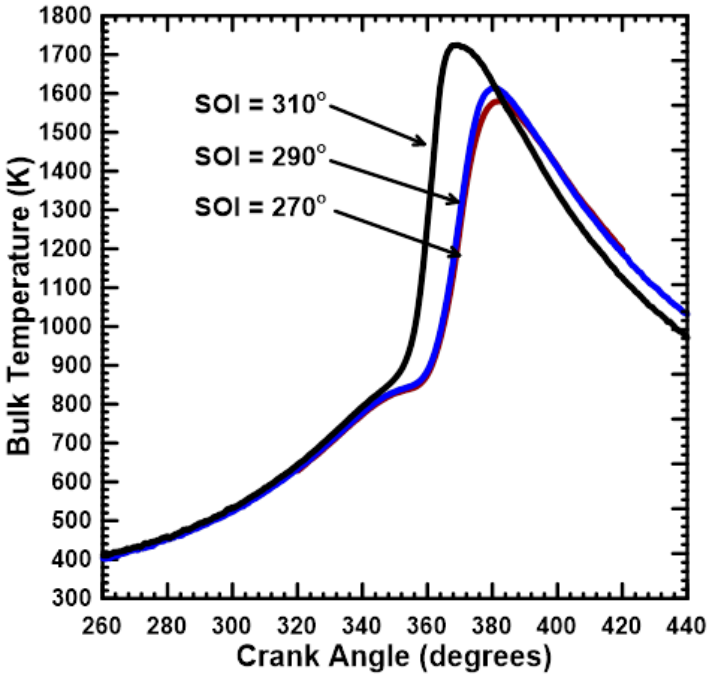

(b)

Figure 3.48 Bulk temperature schedules at (a) late SOIs and (b) advanced SOIs at 12.1 bar IMEP, 95 PES, N=1500 rev/min, P_{in}=1.8 bar

CHAPTER IV

SUMMARY AND CONCLUSIONS

Diesel-ignited methane dual fuel combustion experiments were performed in a single-cylinder research engine. Methane was fumigated upstream of the intake manifold and diesel was injected during the compression stroke with a common rail system. The engine was operated over a range of engine loads from 4.1 bar to 12.1 bar IMEP. Diesel SOI was varied between 360º-260º to study its impact on engine performance and engine-out $ISNO_x$, ISHC, ISCO, and smoke emissions. The results obtained in this study lead to the following conclusions:

- Diesel SOI has a profound effect on performance and emissions characteristics in diesel-ignited methane dual fuel combustion.
- Smoke emissions remain less than 0.05 FSN for all SOIs at each load, likely due to high PES.
- At 4.1 and 6.5 bar IMEP, advancing SOI to 300º reduces $ISNO_x$ to less than 0.15 g/kWh. At 9.5 and 12.1 bar IMEP further advancement of SOI to 280º is required to observe reduced $ISNO_x$. However, $ISNO_x$ levels at 12.1 bar IMEP are higher than those at lower loads, likely due to higher in-cylinder bulk temperatures.

- Very high ISHC and ISCO emissions are observed when SOI is close to TDC. The lowest ISHC and ISCO levels occur at advanced SOI of 310º and earlier. Reduction of ISHC and ISCO at 4.1 bar IMEP to levels observed at higher IMEPs cannot be achieved, likely due to high PES and lower in-cylinder bulk temperatures.
- An increase in IFCE is observed for all loads when SOI is advanced to 310º and earlier. This is likely due to increased combustion efficiency as well as CA50 closer to TDC.
- High MPRR is observed at SOIs between 330º and 320º at lower IMEPs and between 340º and 310º at higher IMEPs. At these SOIs, CA50 occurs before TDC, which leads to high in-cylinder pressures and increased MPRR.

CHAPTER V

RECOMMENDATIONS FOR FUTURE WORK

1. Install an EGR system on the SCRE and repeat these experiments. The effect of EGR on ISNO$_x$ and PM emissions as well as efficiency should be investigated. Furthermore, quantify the effect of EGR on the amount of unburned methane emissions observed during diesel-methane dual fueling.
2. Compare the diesel-methane dual fueling results from this study with other dual fueling cases such as diesel-propane and diesel-gasoline studies performed on the SCRE.
3. Perform optimization studies to determine the "optimal" methane PES at each load with the goal of increasing efficiency and reducing emissions.

REFERENCES

Alzueta, M. U. and Glarborg, P., 2008, “Formation and destruction of CH2O in the exhaust system of a gas engine,” *Environ. Sci. Technol.*, 37, 4512-4516.

Brunt, M. F. J., Rai, H., and Emtage, A. L., 1998, "The calculation of heat release energy from engine cylinder pressure data," *SI Engine Combustion*, SAE Paper No. 981052

Carlucci, A.P., de Risi, A., Laforgia, D., Naccarato, F., 2008, “Experimental investigation and combustion analysis of a direct injection dual-fuel diesel-natural gas engine,” *Energy*, 33, 256-263.

De Carvalho Jr., A. V., 1985, “Natural gas and other alternative fuels for transportation purposes,” *Energy*, 10, 187-215.

Dwivedi, U., 2013, "An experimental investigation of diesel-ignited gasoline and diesel-ignited methane dual fuel concepts in a single cylinder research engine," Thesis, Mississippi State University. Ann Arbor: ProQuest/UMI. (Publication No. ETD-07032013-133320.)

Eng, J.A., 2002, “Characterization of Pressure Waves in HCCI Combustion,” SAE Paper No. 2002-01-2859.

Gatts, T., Shiyu, L., Chetmun, L., Ralston, B., Bell, C., Li, H., 2012, “An experimental investigation of incomplete combustion of gaseous fuels of a heavy-duty diesel engine supplemented with hydrogen and natural gas,” *International Journal of Hydrogen Energy*, 37, 7848-7859.

Gibson, C. M., Polk, A. C., Shoemaker, N. T., Srinivasan, K. K., and Krishnan, S. R., 2011, "Comparison of propane and methane performance and emissions in a turbocharged direct injection dual fuel engine. *Trans. ASME: Journal of Engineering for Gas Turbines and Power*, 133 (9), 092806 (9 pages).

Glassman, I., “Combustion,” 3rd edition, 1996, Academic Press, London, UK.

Hesterberg TW, Lapin CA, Bunn WB, 2008, “A comparison of emissions from vehicles fueled with diesel or compressed natural gas,” *Environmental Science and Technology*, 42, 6437-6445.

Heywood, J.B., 1998, “Internal Combustion Engine Fundamentals,” McGraw Hill, Inc., ISBN 9-78-007028637-5:42-110.

Inagaki, K., Fuyuto, T., Nishikawa, K., and Nakakita, K., and Sakata, I., 2006, “Dual-fuel PCI combustion controlled by in-cylinder stratification of ignitability,” SAE Paper No. 2006-01-0028.

Karim, G. A., 2003, "Combustion in gas fueled compression-ignition engines of the dual fuel type," *Trans. ASME: Journal of Engineering for Gas Turbines and Power*, 125, 827-836.

Kokjohn, S. L., Hanson, R. M., Splitter, D. A., and Reitz, R. D., 2009, “Experiments and Modeling of Dual-Fuel HCCI and PCCI Combustion Using In-Cylinder Fuel Blending,” *SAE Int. J. Engines*, SAE Paper No. 2009-01-2647.

Kokjohn, S. L., Hanson, R. M., Splitter, D. A., and Reitz, R. D., 2011, “Fuel reactivity controlled compression ignition (RCCI): a pathway to controlled high-efficiency clean combustion,” *International Journal of Engine Research*, 12(3), 209-226.

Kolodziej, C., Wissink, M., Splitter, D., Hanson, R. et al., 2013, “Particle size and number emissions from RCCI with direct injections of two fuels,” SAE Paper No. 2013-01-1661.

Korakianitis T, Namasivayam AM, Crookes RJ, 2011, “Natural-gas fueled spark-ignition (SI) and compression-ignition (CI) engine performance and emissions,” *Progress Energy and Combustion Science*, 37, 89-112.

Krishnan, S. R., Srinivasan, K. K., Singh, S., Bell, S. R. et al, 2004, “Strategies for Reduced NOx Emissions in Pilot-Ignited Natural Gas Engines,” *Journal of Engineering for Gas Turbines and Power*, 126(3), 665-671.

Liu, J., Yang, F., Wang, H., Minggao, O., Hau, S., 2013, “Effects of pilot fuel quantity on the emissions characteristics of a CNG/diesel dual fuel engine with optimized pilot injection timing,” *Applied Energy*, 110, 201-206.

Liu, Z., and Karim, G. A., 1995, “The Ignition Delay Period in Dual Fuel Engines,” SAE Paper No. 950466.

Mustafi NN, Raine RR, Verhelst S, 2013, “Combustion and emissions characteristics of a dual fuel engine operated on alternative gaseous fuels,” *Fuel*, 109, 669-678.

Nielsen, O. B., Qvale, B. and Sorensen, S, 1987, “Ignition delay in the dual fuel engine,” SAE Paper No. 870589.

Papagiannakis, R. G. and Hountalas, D. T., 2003, Experimental investigation concerning the effect of natural gas percentage on performance and emissions of a DI dual fuel diesel engine, *Applied Thermal Engineering*, 23(3), 353-365.

Papagiannakis R. G., and Hountalas D. T., 2004, "Combustion and exhaust emission characteristics of a dual fuel compression ignition engine operated with pilot diesel fuel and natural gas," *Energy Conversion Management*, 45(18-19), 2971-2987.

Papagiannakis, R.G., Rakopoulos, C.D., Hountalas, D.T., Rakopoulos, D.C., 2010, "Emission characteristics of high speed, dual fuel, compression ignition engine operating in a wide range of natural gas/diesel fuel proportions," *Fuel*, 89, 1397-1406.

Paul A, Bose PK, Panua RS, Banerjee R, 2013, "An experimental investigation of performance-emission trade off of a CI engine fueled by diesel-compressed natural gas (CNG) and diesel-ethanol blends with CNG enrichment," *Energy*, 55, 787-802.

Polk, A.C., Gibson, C.M., Shoemaker, N.T., Srinivasan, K.K., and Krishnan, S.R., 2013 "Analysis of ignition behavior in a dual fuel turbocharged direct injection engine using propane and methane as primary fuels," *Trans. ASME: Journal of Energy Resources Technology*, 135(3), 032202, (10 pages), (doi:10.1115/1.4023482).

Prikhodko VY, Curran SJ, Barone TL et al., 2011, "Diesel oxidation catalyst control of hydrocarbon aerosols from reactivity controlled compression ignition combustion," In: ASME 2011 international mechanical engineering congress and exposition, Denver, Colorado, USA, 11-17 November 2011, Paper IMECE2011-64147. New York: ASME.

Prikhodko VY, Curran SJ, Barone TL et al., 2010, "Emission characteristics of a diesel engine operating with in-cylinder gasoline and diesel fuel blending," *SAE Int. J. Fuels Lubr.* 3(2), 946-955, SAE Paper No. 2010-01-2266.

Qi. Y, Srinivasan, K. K.,Krishnan, S. R.,Yang, H., et al. 2007, "Effect of hot EGR on the performance and emissions of an advanced injection low pilot-ignited methane engine," *International Journal of Engine Research*, 8(3), 289-303.

Saxena, S., and Bedoya, I. D., 2013, "Fundamental phenomena affecting low temperature combustion and HCCI engines, high load limits and strategies for extending these limits," *Progress in Energy and Combustion Science*, 39(2013), 457-488

Sayin, C and Canaksi, M, 2009, "Effects of injection timing on the engine performance and exhaust emissions of a dual-fuel diesel engine," *Energy Conversion and Management*, 50(1), 203-213.

Selim, MYE, 2001, "Pressure-time characteristics in diesel engine fuelled with natural gas," *Renewable Energy*, 22(4), 473-489.

Shah S.D., Johnson K.C., Miller J.W., Cocker D.R., 2006, “Emissions rates of regulated pollutants from on-road heavy-duty diesel vehicles,” *Atmospheric Environment*, 40, 147-153.

Splitter, D. A., Hanson, R. M., Kokjohn, S. L., and Reitz, R. D., 2011, “Reactivity controlled compression ignition (RCCI) engine operation at mid and high loads with conventional and alternative fuels,” SAE Paper No. 2011-01-0363.

Srinivasan, K. K.,Krishnan, S. R., Singh, S., Midkiff, K.C., et al, 2004, “The Advanced Low Pilot Ignited Natural Gas Engine – A Combustion Analysis,” *Journal of Engineering for Gas Turbines and Power*,128(1), 213-218.

Srinivasan, K. K., Krishnan, S. R., Midkiff, K. C., 2006, “Improving low load combustion, stability and emissions in pilot-ignited methane engines,” *Proc. IMechE: Journal of Automobile Engineering*, Part D, 220(2), 229-239.

Srinivasan, K.K.,Krishnan, S. R., Qi, Y., Yang, H., Midkiff, K.C., 2007, "Analysis of diesel pilot-ignited methane low-temperature combustion with hot exhaust gas recirculation," *Combustion Science and Technology*, 179(9), 1737-1776.

US EPA Heavy-Duty Engine Emissions standards: http://www.dieselnet.com/standards/us/hd/php; accessed on January 31, 2013.

Yao, M., Zheng, Z., Liu, H., 2009, “Progress and recent trends in homogeneous charge compression ignition (HCCI) engines,” *Progress in Energy and Combustion Science*, 35, 398-437.

Zhou, L., Liu, Y.-F., Wu, C.-B., Sun, L. et al., 2013, “Effect of the diesel injection timing and the pilot quantity on the combustion characteristics and the fine-particle emissions in a micro-diesel pilot-ignited natural-gas engine,” *Proc. IMechE, Part D: J. Auto Engg.*, 227(8): 1142-1152